Druppel, K., Littmann, S., Romer, R. L., Okrusch, M. (2007): Petrology and isotope geochemistry of the Mesoproterozoic anorthosite and related rocks of the Kunene. Intrusive Complex, NW Namibia. - Precambrian Research, 156, 1-2, 1-31,

DOI: 10.1016/j.precamres.2007.02.005.

Petrology and isotope geochemistry of the Mesoproterozoic anorthosite and related rocks of the Mesoproterozoic Kunene Intrusive Complex, NW Namibia

K. Drüppel[a*], S. Littmann[b], R.L. Romer[b], M. Okrusch[c]

[a] *TU Berlin, Abteilung Mineralogie, Sekr. ACK9, Ackerstr. 71-76, D-13355 Berlin, Germany*

[b] *GeoForschungsZentrum Potsdam, Am Telegraphenberg, D-14473 Potsdam, Germany*

[c] *Universität Würzburg, Institut für Mineralogie, Am Hubland, D-97074 Würzburg, Germany*

*Corresponding author. Present address: Technische Universität Berlin, Institut für Angewandte Geowissenschaften, Abteilung Mineralogie, Sekr. ACK9, Ackerstr. 71-76, D-13355 Berlin, Germany.

Telephone: +49-(0)30-314-72083. Fax: +49-(0)30-314-72218.

E-mail address: kirsten.drueppel@tu-berlin.de

Abstract

The intrusion of the large (c. 18.000 km^2) anorthosite body of the Kunene Intrusive Complex, Angola/Namibia, which is associated with minor marginal granite bodies and syenite/syenodiorite dykes, marked the beginning of Mesoproterozoic igneous activity in NW Namibia. Anorthosites display an igneous mineral assemblage of dominating plagioclase, together with minor olivine, orthopyroxene or clinopyroxene, Fe-Ti oxides, whereas biotite and pargasite are late-magmatic phases. Apatite is a common accessory phase. In regionally associated felsic rocks K-feldspar, plagioclase, clinopyroxene and/or hastingsite crystallized first, followed by interstitial quartz, hastingsite, Fe-Ti oxides, and titanite. The general geochemical characteristics for the anorthositic rocks of the Kunene Intrusive Complex (i.e. high Al_2O_3, CaO, Sr and Eu, intermediate to high Mg numbers of 0.37-0.74, positive εNd (T) values of +3.0 to +1.0, and initial Sr ratios of 0.7028-0.7041) are in excellent agreement with their derivation from fractionated basaltic liquids. The $\delta^{18}O$ values obtained for plagioclase (5.88 ± 0.19 ‰ $\delta^{18}O$) support their development from mantle-derived magmas. Relic crustal xenoliths of calc-silicate rocks and Sr and Nd isotope data, however, suggest that the anorthosite magma underwent minor crustal contamination, which was most prominent during the early intrusion stage. A U-Pb-zircon age of 1376 ± 2 Ma was obtained for a felsic rock associated with the 1385 ± 25 Ma anorthosites, which suggests that the two suites were emplaced during the same igneous event. The geochemical and isotope signatures of the granites, syenites, and syenodiorites provide convincing evidence against consanguinity of the anorthositic and the felsic rock suites, i.e.: (1) a compositional gap exists between the major and trace element contents of the two suites, (2) trace element and Sr, and Nd isotopic data of the felsic rocks point to a crustal source (εNd: +2.0 to -0.4, initial Sr ratio: 0.7024-0.7063), (3) the REE patterns of the felsic rocks do not exhibit ubiquitous negative Eu-anomalies, which

would be expected from fractionation products of melts that previously formed extensive plagioclase cumulates, and (4) $\delta^{18}O$ values of magmatic feldspar from the felsic rock suite fall in a restricted range (7.20-7.92 ‰) that is about 1.6 ‰ higher than the average igneous plagioclase $\delta^{18}O$ of the anorthosites and suggests a formation of the felsic melts by anatexis of the lower crust.

Keywords: Congo Craton, felsic rocks, isotope geochemistry, leuconorite, leucotroctolite, oxygen isotopes.

1. Introduction

Massif-type anorthosite complexes, commonly associated with minor volumes of mafic and granitic rocks, are characteristic features of the Proterozoic crust. Their apparent temporal restriction to the Proterozoic suggests that specific tectono-thermal regimes and crust-forming processes have been operative during this period. Many anorthosite massifs underwent a prograde amphibolite to granulite facies metamorphism after their emplacement, which complicates the reconstruction of their magmatic evolution. Thus, the petrogenesis of Proterozoic anorthosite complexes is still a matter of debate. No general agreement has been reached on issues such as the source of parental magmas of the anorthosite and granite suites, monobaric *vs.* polybaric anorthosite crystallization, mode and depth of emplacement and cooling history (*e.g.* Ashwal, 1993, for a review).

In general, the petrogenesis of the huge anorthosite massifs is interpreted in terms of partial melting of the upper mantle, followed by plagioclase flotation in a magma chamber at the mantle-crust boundary and buoyant ascent of the plagioclase-rich crystal mushes to their final depth of emplacement (Duchesne, 1984; Emslie, 1985, Emslie et al., 1994; Longhi and Ashwal, 1985; Ashwal, 1993; Wiebe, 1994; Mitchell et al., 1995). Recently, however, many authors favour the hypothesis of anorthosite generation by lower crustal anatexis (Taylor et al., 1984; Duchesne et al., 1999; Longhi et al., 1999; Schiellerup et al., 2000; Selbekk et al., 2000, Wiszniewska et al., 2002), which is supported by Re-Os isotope data and experimental investigations. With the results presented here we contribute new data to this debate.

Most anorthosite massifs contain a considerable volume of temporally and spatially associated granitic plutonic rocks, characterized by a composition ranging from diorite to granite and a mostly anhydrous mineralogy. Commonly, intrusive contact relationships suggest these granitoids to be younger than the associated anorthosite (e.g. de Waard, 1970;

Seifert, 1978). The fact, that the mineral chemistry of the Fe-Mg silicates and plagioclase in the silicic suites appears to extend the compositional ranges of the anorthositic minerals to higher X_{Fe} and lower An-contents, respectively, has been interpreted in terms of consanguinity between the two rock suites (e.g. Fuhrman et al., 1988). An alternative model considers the granitoids to represent a chemically independent, crustal derived intrusive suite (e.g. Anderson, 1980; Anderson & Bender, 1989; Emslie, 1991; Emslie et al., 1994).

Among the anorthosite bodies of the world, the Kunene Intrusive Complex (KIC), NW Namibia, and the Lac-Saint-Jean Complex, Canada, are presumably the largest exposed massifs, both covering a total surface area of *c.* 18,000 km^2. Nonetheless, the Kunene Intrusive Complex is one of the least known anorthosite bodies of the world. In clear contrast to most anorthosite bodies world-wide, the Mesoproterozoic KIC experienced no prograde metamorphic overprint after its emplacement (e.g. Ashwal and Twist, 1994; Morais et al., 1998; Drüppel, 1999, 2003; Drüppel et al., 2001; Slejko et al., 2002; Mayer et al., 2004) and hence allows direct study of the igneous processes that led to its formation.

We describe and interpret the mineralogical and geochemical signatures and Nd, Sr, and O isotope data from the anorthositic rocks of the Kunene Intrusive Complex and the associated granitoid suite and provide a U-Pb zircon age for the emplacement of the associated syenites. Our results place constraints on the tectono-metamorphic evolution of the Congo Craton during the Proterozoic and on some aspects of the petrogenesis of massif-type anorthosites in general.

2. Geological framework

Anorthositic rocks of the Kunene Intrusive Complex (KIC) cover an estimated surface area of 18,000 km^2 in NW Namibia and SW Angola and are regarded to form one of the

largest massif-type anorthosite bodies in the world (e.g. Ashwal and Twist, 1994; Morais et al., 1998; Drüppel et al., 2001; Mayer et al., 2004). The anorthosite massif was emplaced at the southern margin of the Congo Craton in the Mesoproterozoic. In Namibia, the KIC intruded the high-grade metamorphic rocks of the Epupa Complex, which mainly consists of upper amphibolite facies rocks of the Orue Unit, comprising migmatitic granitic orthogneisses and subordinate migmatitic metasedimentary and metavolcanic rocks (Brandt, 2003; Brandt et al., 2003). South of the KIC, two limited areas of ultrahigh-temperature granulite-facies rocks, the Epembe Unit, have been recognized by Brandt et al. (2003, 2007), that mainly consist of a volcano-sedimentary sequence of interlayered felsic and mafic granulites, intercalated with subordinate migmatitic metasediments that contain rare lenses of sapphirine-bearing granulites (Brandt et al., 2003, 2007). The Epembe Unit is separated from the Orue Unit by subvertical ductile shear zones. Both units preserve Palaeoproterozoic protolith ages (Seth et al., 2003, 2005), that were also recognized in other parts of the Epupa Complex and the Congo craton (see reviews in Tegtmeier and Kröner, 1985; Carvalho et al., 2000). SHRIMP U-Pb zircon dating of granulite facies rocks from the Epembe Unit reveals Mesoproterozoic ages between 1520 Ma and 1510 Ma for prograde zircon growth under granulite-facies conditions, whereas slightly younger Pb-Pb garnet ages of 1450 ± 50 Ma date the peak of UHT metamorphism (Seth et al., 2003). Distinctly younger Pb-Pb garnet and U-Pb SHRIMP ages of zircon rims of 1340-1320 Ma have been recorded for part of the amphibolite facies rocks of the Orue Unit by Seth et al. (2005).

Rarely exposed contacts between the KIC and the metamorphic basement are largely obliterated by broad ductile shear zones and late brittle faults, which were subsequently intruded by syenite and/or dolerite dykes. Direct intrusion contacts are only observed between the white anorthosite and the amphibolite facies Orue Unit at the southeastern margin of the KIC. Along this contact zone, a narrow contact-thermal aureole of several metres in width is

developed in the Orue Unit, which is recorded by Grt-Crd-Sill hornfelses (Brandt, 2003; Brandt et al., 2003). For this rock a Pb-Pb garnet age of 1341 ± 47 Ma Ma has been recorded (Seth et al., 2005).

At least two major anorthosite units can be distinguished, separated by a NE-SW trending belt of granitoid intrusions (Morais et al., 1998; Drüppel et al., 2001; Fig. 1):

(1) The majority of the KIC exposed in Angola displays a N-S elongation and is mainly composed of dark, weakly altered anorthositic rocks (mainly anorthosites and leucotroctolites; *e.g.* Carvalho and Alves, 1990, Silva, 1990, 1992, Ashwal and Twist, 1994, Morais et al., 1998, Slejko et al., 2002, Mayer et al., 2004). Based on satellite images Ashwal & Twist (1994) concluded that even this northern part of the KIC represents a composite massif, composed of at least eight separate anorthosite plutons. A similar interpretation has also been reached by Morais et al. (1998) and Slejko et al. (2002), who distinguished at least two individual anorthosite bodies in the Angolan part of the KIC, a northern and a southern zone, that display remarkable differences in their geochemical characteristics and mineralogy.

(3) The southernmost KIC, on the other hand, including the study area in Namibia (Fig. 1, 2), has a pronounced E-W elongation. In this area the KIC mainly consists of heavily tectonised and pervasively altered pale anorthosite, the ‘white anorthosite’ (*cf.* Köstlin, 1967, 1974, Menge, 1998, Drüppel et al., 2001). The coarse white anorthosite is characterised by a white or pale violet and greenish colour and comprises anorthosites *senso stricto* as well as leuconorites with abundant orthopyroxene of up to 8 cm in diameter. This white anorthosite massif is intruded by subordinate, sheet-like bodies of dark, weakly altered anorthosites, leucogabbronorites and leucotroctolites ('dark anorthosite') that typically contain xenoliths of the white anorthosite. Anorthosites and leucogabbronorites of the dark anorthosite suite mainly occur in the centre of the white anorthosite massif, forming the Zebra Mountains, and

grade into small bodies of leucotroctolite and olivine-bearing anorthosite towards the margin of the KIC. Cumulate textures are relatively widespread on a local scale; yet no evidence for extensive layering or igneous lamination was recognized, in contrast to the interpretation of aerial photographs by Menge (1996, 1998). If transected by major faults dark anorthosite is always strongly sericitised and can then be easily confused with the white anorthosite. Towards the north, the dark anorthosite massif is terminated by a major NE trending, ca. 6 km wide dextral shear zone, the 'Serpa Pinto Lineament' of Menge, 1998, which is partly intruded by small dark anorthosite bodies. Along this major fault bundle the white anorthosite is strongly tectonized and partly intermingled with structurally isolated and incorporated blocks of the Orue Unit (Fig. 2).

For the emplacement of the KIC at the southern margin of the Congo craton, an internal biotite-plagioclase whole-rock Rb-Sr isochron date of 1347 ± 13 Ma has been determined for an anorthosite sample of the northern Angolan part of the complex (Mayer et al., 2000). This age has been superseded by an almost concordant U-Pb age of 1371 ± 2.5 Ma using zircons from a cogenetic mangerite vein (Mayer et al., 2004). The latter age is in accordance with a preliminary, subconcordant U/Pb single-zircon age of 1385 ± 25 Ma, obtained for a leucogabbronorite sample of the dark anorthosite suite from Namibia (Drüppel et al., 2000). A Sm-Nd mineral (amphibole-biotite-plagioclase-pyroxene) bulk rock age of 1319 ± 13 Ma, determined on an Angolan anorthosite, marks the end of the anorthosite activity (Mayer et al., 2004). Radiometric dates for the white anorthosite are lacking, so far. The age of the emplacement and cooling of the KIC between *c.* 1385 and 1319 Ma covers the ages of both contact metamorphism at ca. 1341 Ma and the regional metamorphic overprint of the Orue Unit at 1340-1320 Ma, suggesting that the emplacement of the anorthositic magma had a regional thermal effect on the bordering Orue Unit.

Massive Fe-Ti ore bodies have been reported from all parts of the KIC (e.g. Morais et al., 1998, von Seckendorff et al., 2000) but are, in our study area, largely restricted to the white anorthosite. Several small mafic (gabbro) and ultramafic bodies (pyroxenite, hyperite, peridotite) which are inferred to be genetically related to the KIC, crop out within the basement near the contact to the KIC (Fig. 2). Close to its southernmost margin, the Namibian KIC as well as the neighbouring basement are transected by numerous SE and NE trending felsic dykes (mainly alkali granites, syenites, syenodiorites). These felsic intrusives may be subdivided into two units (Fig. 2): (1) an older generation of mainly ENE trending bodies of up to 40 km long and 2-3 km wide is exposed in the Epupa Complex and (2) a second generation of mainly NW trending dykes exposed over 100 m in length and 3-10 m in width are observed exclusively within the marginal zones of the KIC. The emplacement of the felsic rocks in both areas may be related to regional granitic magmatism in NW Namibia in the Mesoproterozoic, i.e. the granite belt that separates the northern and southern part of the KIC (Rb-Sr whole-rock isochrons of 1411-1302 Ma: Torquato et al., 1979) and mangerite veins in anorthosite in Angola (U/Pb single-zircon age of 1371 ± 2.5 Ma: Mayer et al., 2004). Near the southern margin of the KIC, the basement rocks are intruded by several nepheline syenite stocks with U-Pb zircon ages of ca. 1216-1213 Ma (Littmann et al., 2000; Fig. 2) In the southeastern part of the KIC, in the Swartbooisdrif area, the subsequent emplacement of ca. 1140 Ma ferrocarbonatites as dykes was locally responsible for a local but pervasive fenitisation of the older felsic rocks (Drüppel et al., 2005).

3. Analytical methods

All electron microprobe analyses reported here were performed on a CAMECA SX50 instrument, with three WDS spectrometers, housed in the Institute of Mineralogy, University

of Würzburg or on a CAMECA SX50 and SX100 at the GeoForschungsZentrum Potsdam (GFZ). Operating conditions were 15 kV accelerating voltage and 15 nA beam current with 1-5 μm spot size of Würzburg and 20 nA beam current with 2-5 μm for amphibole, pyroxene, epidote and magnetite/ilmenite to 10 μm for feldspar at the GFZ Potsdam. The accessory minerals apatite and zircon were measured with an accelerating voltage of 20 kV, using a beam current of 10 nA for apatite and 40 nA for zircon at the GFZ Potsdam.

The X-ray fluorescence (XRF) analyses of the major and trace element content anorthositic and granitic rocks were determined from fused glass discs with a Philips PW 1480 XRF spectrometer at the Institute of Mineralogy, Würzburg. Matrix effects were corrected automatically by the Philips X40 software. The relative analytical error for major and trace elements is 1 % and 1-8 %, respectively. FeO contents were analysed using a ZEISS PMD 2 spectral photometer.

Additional trace elements of selected samples were analysed by Inductively Coupled Plasma Mass Spectrometry (ICP-MS) using a VG Plasma Quad PQ^{2+} at the GFZ Potsdam, Germany. Sample powders were digested in HF-$HClO_4$, dried and then redissolved in dilute HNO_3. Calibration was carried out using multi-element solutions and routinely checked for accuracy with international geological reference materials. Precision is generally better than ± 10% (rel.) for each element (Plessen, 1997).

Rare earth element analyses were carried out at the GFZ Potsdam. Sample preparation followed the method of Zuleger and Erzinger (1988). Measurements of REE and Y concentrations were conducted by ICP-AES. Details on ICP equipment, operating conditions, background wavelength corrections and background equivalent concentrations as well as precision of the method are given in Zuleger and Erzinger (1988).

Stable isotope ratios are reported for hand-picked mineral separates of feldspar. The silicates were treated with ClF_3 according to the method described by Borthwick and Harmon

(1982) at the Geochemical Institute, University of Göttingen. All $\delta^{18}O$ values are given relative to SMOW. The reproducibility of $\delta^{18}O$ values is better than ± 0.2 ‰.

The Sr and Nd isotope composition of the whole rock samples was determined at the GFZ Potsdam. The whole rock powders were dissolved in HF on a hot plate (160°C). After drying, residues were redissolved in 6N HCl and split for the determination of the isotopic composition (IC) and for concentration determination by isotope dilution (ID). The ID splits were spiked with ^{87}Rb-^{84}Sr tracer and a ^{150}Nd-^{149}Sm tracer. Strontium and rubidium were analysed on Ta filaments using a VG Sector 54-30 mass spectrometer and neodymium and samarium were analysed with a Finnigan MAT 262 mass spectrometer on Re filaments. All Sr ratios were normalized to $^{86}Sr/^{88}Sr = 0.1194$. The average value for $^{87}Sr/^{86}Sr$ obtained from NBS SRM 987 standard during the period of this study was 0.710246 ± 10 (2σ, n = 20 independet measurements). Mass fractionation for Nd and Sm was corrected by normalizing to $^{146}Nd/^{144}Nd = 0.7219$ and $^{147}Sm/^{152}Sm = 0.5608$, respectively. Repeated analysis of the La Jolla standard yielded a value of $^{143}Nd/^{144}Nd = 0.511855 \pm 8$ (2σ, n = 15 independent measurements). For details see Romer et al. (2005). Initial Sr and Nd isotopic ratios were calculated using Rb/Sr and Sm/Nd ratios determined by isotope dilution.

Zircon was used for the U-Pb age determination of the syenite suite at the GFZ Potsdam. The zircon separates were produced using Wilfley table, heavy liquids, and Frantz isodynamic magnetic separator. Concentrates were purified by hand under the binocular microscope. The individual analyses were performed on euhedral, unbroken crystals. A mixed ^{205}Pb-^{235}U tracer was added before sample dissolution in HF. The samples were dissolved in teflon capsules in a Parr® autoclave at 220°C for four days. After drying the samples on the hot plate, samples were taken up in 6N HCl and redissolved overnight in the Parr® autoclave at 220°C. U and Pb were separated using the ion-exchange chromatography of Krogh (1973). Pb and U were loaded together with colloidal silica and H_3PO_4 on a single Re-filament. The isotope ratios for

Pb and U were determined at 1200-1260°C and 1300-1560°C, respectively, on a Finnigan MAT 262 multi-collector mass spectrometer using an ion-counter and Faraday collectors. Analytical precisions on the 2σ level, including uncertainties for the mass fractionation, are generally better than 0.1%, except for ratios involving ^{204}Pb. The total procedure blanks were 5 to 10 pg for Pb and below 1 pg for U. Ages were calculated using the constants recommended by IUGS (Steiger and Jäger, 1977).

4. Petrography and Mineral Chemistry

Data on the mineral chemistry of selected minerals were obtained for 20 rock samples out of a total of 67 samples of the anorthosite suite and 6 rock samples out of 57 samples of the granite-syenite suite. Representative analyses of feldspar, pyroxene and amphibole are compiled in Tables 1 to 3. The full set of EMP analyses is given in Drüppel (2003) and may be obtained from the first author, on request.

4.1. Anorthositic rocks

The petrography and mineral chemistry of the anorthositic rocks of the KIC were discussed in some detail by Drüppel et al. (2001). The authors have shown that both the white and the dark anorthosite suite display the primary magmatic assemblage of cumulus plagioclase (An_{43-53} and An_{43-75}, respectively) ± olivine ± orthopyroxene ± clinopyroxene ± biotite ± pargasite/magnesio-hastingsite + ilmenite + magnetite ± apatite ± zircon ± sulfides.

Crustal xenoliths are represented by relic xenocrysts of andradite-rich garnet (average composition: $Adr_{72}Grs_{27}$), which are exclusively observed in samples of white anorthosite and

in leucogabbronorite of the dark anorthosite suite. The fractured garnet grains are partially replaced by chlorite and surrounded by late-magmatic pargasite. The mineralogical compositions of the xenoliths point to a contamination of the parental melt with calc-silicate gneisses of the country rock.

4.1.1 White anorthosite

White anorthosite represents the first recognisable generation of anorthosite magmatism. A characteristic feature of the white anorthosite is the dominance of coarse (commonly 1-5 cm in diameter), anhedral cumulus plagioclase (87-99 vol.%). Plagioclase crystals commonly display embayed grain boundaries and suffered an almost complete hydrothermal alteration (i.e., saussuritisation, albitisation and/or sericitisation), responsible for the white to pale violet or greenish colour of these rocks. Unaltered plagioclase relicts (An_{43-53}) mostly exhibit a weak normal or oscillatory zoning with an average An-decreases from core to rim of about 2 mol.%.

Cumulus to interstitial orthopyroxene (X_{Mg}: 0.71), in cases forming orthopyroxene-megacrysts of up to 8 cm in diameter, is the main Fe-Mg silicate present in the leuconorites and is commonly completely replaced by chlorite that encloses preserved ilmenite exsolution lamellae. Accessory intercumulus clinopyroxene is always completely replaced by late actinolite and enveloped by a narrow rim of late-magmatic pargasite (Al p.f.u.: 2.42-2.97; X_{Mg}: 0.65-0.70; Table 3). Magnetite and ilmenite are minor constituents of the white anorthosite and occur as discrete anhedral grains in the interstices of cumulus plagioclase. Olivine or its alteration products have not been observed in the investigated samples.

Small-scaled ductile shear zones transect part of the samples. Locally, plagioclase is strongly deformed or even recrystallised to granular mosaics of inversely zoned albite (An_{3-4}

to An_{5-10}), that presumably formed during the hydrothermal alteration of the rocks. Late cracks are filled by carbonate and/or epidote.

4.1.2 Dark anorthosite

In the subsequently emplaced dark anorthosite suite subhedral tabular coarse-grained (commonly 0.5-3 cm in diameter) cumulus plagioclase is the dominant mineral (65-99 vol.%). The vast majority of the analysed plagioclase crystals display minor chemical zoning, with the anorthite contents falling in the compositional range of andesine to labradorite (An_{43-75}; Table 1). The An-contents of plagioclase increase in the sequence (1) leucogabbro/pyroxene anorthosite (An_{43-54}), (2) leucotroctolite/olivine anorthosite (An_{47-60}), and (3) garnet-bearing leucotroctolite (An_{55-75}). Minor orthopyroxene and clinopyroxene are the dominant mafic minerals (3-12 vol.%) in the leucogabbronorite samples (Fig. 3a). They occur as large, subhedral to anhedral cumulus to intercumulus phases or form rims around olivine. Following the IMA-classification (Morimoto, 1988) clinopyroxene of the leucogabbronorites ($Wo_{44.4}En_{32.6}Fs_{18.3}$ – $Wo_{45.7}En_{27.8}Fs_{20.7}$) and leucotroctolites ($Wo_{40.03}En_{34.4}Fs_{21.5}$ – $Wo_{45.7}En_{39.1}Fs_{12.3}$) is diopside and subordinately augite (Table 2). The Al_2O_3 content of clinopyroxene increases from leucogabbronorite (1.5-1.9 wt.%) to leucotroctolite (1.7-3.3 wt.%). Orthopyroxene of the anorthositic suite is enstatite with high X_{Mg} (0.54-0.63) but with lower Al_2O_3 contents (0.4-1.8 wt.%; Table 2). In the olivine anorthosite and leucotroctolite subordinate olivine (5-8 vol.%; X_{Mg}:0.54-0.65) occurs as small subhedral inclusions in plagioclase or as large, subhedral to anhedral, interstitial grains, partially rimmed by pyroxene (Fig. 3a, 3b). Magnetite is observed as minute inclusions in plagioclase and olivine, or, together with ilmenite, as large, anhedral grains in the interstices between plagioclase crystals (up to 3 vol.%). Especially in the leucogabbronorite, both, ilmenite and pyroxene are surrounded by narrow rims of late-magmatic biotite (X_{Mg}: 0.39-0.67) and amphibole. The vast

majority of late-magmatic amphibole of the leucogabbronorite and pyroxene anorthosite of the dark anorthosite suite is magnesio-hastingsite/pargasite to ferro-pargasite/hastingsite (Al p.f.u.: 1.82-2.51; X_{Mg}: 0.46-0.73; Table 3). Anorthosite *senso stricto* contains only minor amounts of Mg-Fe silicates and Fe-Ti oxides (0.5-3 vol.%). Zircon is extremely rare and has only been observed in two of the 67 investigated anorthosite samples. Apatite is commonly present as an accessory phase in the leucogabbronorites, where it occurs as inclusions in the late-magmatic amphibole and biotite. In some leucotroctolite samples garnet-bearing corona textures are developed around olivine and Fe-Ti oxides (Drüppel et al., 2001).

4.2. Felsic rock suite

The felsic rocks are characterised by a coarse equigranular, massive appearance. A weak foliation is exclusively developed in the marginal zones of the large granite bodies in the basement and is attributed to syn-emplacement deformation. Small felsic dykes transecting the KIC, on the other hand, locally show igneous lamination, defined by a preferred orientation of feldspar. The samples investigated are mainly composed of subhedral to anhedral, tabular alkali feldspar (55-75 vol.%; microcline and occasional orthoclase: Or_{91-98}), displaying strong micro- to mesoperthitic albite exsolution (An_{1-4}; Fig. 3c). Reintegrated compositions of alkali feldspar cores fall in the range of $Ab_{43.3}An_{1.9}Or_{54.8}$ – $Ab_{85.8}An_{4.1}Or_{10.1}$ whereas the feldspar rims have a more albite-rich composition ($Ab_{86.8}An_{2.6}Or_{10.6}$ – $Ab_{88.3}An_{3.1}Or_{8.6}$) or are the almost pure albite end member (Ab_{95-99}). String perthite, transgressing into patch and block perthite is most common, whereas other exsolution textures like braid, vein, plate or flame perthite are rare. A second generation of later microcline may occur, forming separate, anhedral grains that lack exsolution textures. Sericitization is concentrated in the crystal cores. Platy plagioclase with weak reverse zonation (An_{9-18}; Table

1), showing mostly subhedral to euhedral shape occurs in variable amounts (5-35 vol.%), but is always less abundant than alkali feldspar. Secondary albite, grown at the expense of alkali feldspar, exhibits a weak normal zonation (An_{4-5} to An_{0-2}) or is the unzoned, almost pure albite end member. In some of the samples that underwent hydrothermal alteration secondary albite may be present in significant amounts of > 50 vol.%.

The dominant mineral among the Fe-Mg silicates (5-23 vol.%) in most of the felsic rock samples is hastingsite, which is either enclosed by plagioclase or fills interstices between individual feldspar crystals. Amphibole of both textures displays low Al and X_{Mg} (Al p.f.u.: 1.91-2.10; X_{Mg}: 0.01-0.06) when compared to amphibole of the anorthosite suite (Table 3). In quartz-poor or -free samples greenish clinopyroxene (3-8 vol.%; X_{Mg}: 0.45-0.51) may be present, which fills interstices between feldspar crystals (Fig. 3d), but may also occur as inclusions in feldspar. The clinopyroxene is generally more hedenbergitic in composition ($Wo_{43.8}En_{23.1}Fs_{28.0}$ – $Wo_{45.1}En_{25.4}Fs_{24.3}$) when compared to that of the anorthositic rocks (Table 2). Its Al_2O_3 contents are low (0.4-0.8 wt.%), reflecting the Al-poor whole-rock composition of the rocks. In most samples clinopyroxene is partially to completely replaced by fibrous ferro-hornblende to ferro-actinolite (X_{Mg}: 0.23-0.31). Anhedral magnetite, either spatially associated with ilmenite or displaying oxidative exsolution of ilmenite after lamellae as well as anhedral quartz (granite 13-25 vol.%, quartz-bearing syenodiorite: 5-8 vol.%) fill interstices between feldspar crystals. Titanite (aTtn: 0.87-0.90), forming large anhedral grains or as rims around Fe-Ti oxides, is the most common accessory phase, associated with euhedral zircon. Apatite occurs as stubby prisms, commonly enclosed by plagioclase.

Secondary enrichment of epidote (Ps_{21-34}), locally associated by carbonate and/or chlorite (X_{Mg}: 0.09-0.11), is common in samples, where hydrothermal alteration is more pronounced. A conspicuous feature are symplectitic intergrowths of green hastingsite (X_{Mg}: 0.01-0.06), plagioclase (An_{9-18}), ilmenite and magnetite replacing interstitial hastingsite.

5. Geochemical characteristics

Major and trace element geochemical data were obtained for 56 rock samples of the anorthosite suite and 33 rock samples of the granitoid suite. Representative analyses of the major and trace element data and of the REE data are compiled in Tables 4 and 5, respectively. The full set of analyses is given in Drüppel (2003) and may be obtained from the first author, on request.

5.1. Anorthositic rocks

Both the white and the dark anorthosite suite are rich in Al_2O_3 (21-29 and 16-30 wt.%), SiO_2 (45-51 and 38-54 wt.%), CaO (4-13 and 7-13 wt.%), and Na_2O (4-9 and 3-6 wt.%), reflecting high amounts of plagioclase, whereas they are deficient in all other oxides (Fig. 4). The $Fe^{tot}/(Fe^{tot}+Mg)$ ratio is > 0.28, pointing to anorthosite crystallization from a fractionated melt (Fig. 5). The highest average $Fe^{tot}/(Fe^{tot}+Mg)$ values occur in the white anorthosite (0.51-0.74) and leucogabbronorite of the dark anorthosite suite (0.31-0.66). The geochemical trends of the major elements of the least altered samples of the dark anorthosite suite, as demonstrated in various Harker diagrams, correlate well with varying modal proportions of plagioclase and Fe-Mg silicates and Fe-Ti oxides and are hence unlikely to reflect different degrees of fractionation. Decreases of Si, Al, Ca, and Na are accompanied by increases of Fe, Mn and Mg from anorthosite and troctolite towards leucogabbronorite of the dark anorthosite suite (Fig. 4, 5). Leucogabbronorites generally display the highest values of K and P, reflecting generally high amounts of late-magmatic biotite and apatite, which crystallized from pockets of intercumulus melt. Trends of the white anorthosite are mostly

indistinguishable from those of the dark anorthosite suite, with the exception of Na and K that were apparently strongly enriched during the hydrothermal alteration.

The highest values for Ni are obtained for olivine-bearing rock samples, whereas the high V and Zn values of the leucogabbronorites are reflected by higher modes of ilmenite and pyroxene. The highest Sr concentrations have been obtained for white anorthosite and pyroxene anorthosite/leucogabbronorite of the dark anorthosite suite, which also exhibit the highest overall trace element abundances. Regarding their rare earth element patterns, all anorthositic rocks are characterized by a variable enrichment of the light REE (La_N/Yb_N: 3.3-26.9), a strong positive Eu (Eu/Eu*: 1.3-11.2) anomaly and flattening in the heavy REE (Fig. 6), typical of plagioclase cumulate rocks. In the dark anorthosite, the overall abundance of REE increases in the sequence leucotroctolite/olivine-bearing anorthosite towards pyroxene-bearing anorthosite/leucogabbronorite, resulting in a relative decrease of the Eu anomaly. The overall increase of the REE can be partly explained by a higher modal abundance of apatite in the leucogabbronorite. The white anorthosite shows strongly varying REE patterns, one (Ku-97-45; Eu/Eu*: 7.1¸ La_N/Yb_N: 26.9) resembling that of the leucotroctolites of the dark anorthosite suite whereas two other patterns (Ku-98-44, Ku-97-33b; Eu/Eu*: 1.6-2.3; La_N/Yb_N: 5.9-12.6) agree well with those of the leucogabbronorites and pyroxene anorthosites. It may thus be concluded that the white anorthosite, like the dark anorthosite, is not only composed of anorthosites *senso stricto* as was proposed by Menge (1998) but also comprises leucotroctolites and leucogabbronorites. When compared to the corresponding lithologies of the dark anorthosite suite, all three white anorthosite samples display a slight enrichment in the light REE and a relative decrease of the heavy REE, indicating either an elevated amount of crustal contamination or a later alteration of the rocks.

The major and trace element data of the anorthosite suite permit comparison with large Proterozoic anorthosite massifs of N America, like Harp Lake, Marcy, Nain, and Lac Saint-

Jean (see Ashwal, 1993, for a review; Fig. 5). When compared to the anorthosites investigated in the Angolan part of the KIC (Morais et al., 1998), the Namibian rock suite is characterised by a similar variability of geochemical compositions but higher average amounts of Na_2O.

5.2. Felsic rock suite

The geochemical characteristics of the felsic rock suite have been investigated for dykes transecting both the basement and the KIC. The SiO_2 contents of the felsic rocks exposed in the basement range between 71-76 wt.%, whereas those of the dykes transecting the anorthositic KIC are distinctly lower (51-66 wt.%). According to the classification of Cox et al. (1979; Fig. 7), the granitic bodies intruding the basement can be classified as alkali granites to granites, whereas the felsic dykes transecting the anorthositic KIC are syenites and syenodiorites. The syenites/syenodiorites are either slightly quartz-normative or slightly nepheline-normative. Quartz-normative syenite and syenodiorite samples can be classified as jotunites to mangerites, whereas the granites resemble charnockites following the nomenclature of Streckeisen (1974) for charnockitic rocks that is often adopted for felsic rock suites associated with anorthosite massifs.

Samples of the felsic rock suite are generally enriched in K_2O (1.3-5.8 wt.%) and/or Na_2O (3.6-8.3 wt.%) relative to CaO (<5.9 wt.%, except for Ku-98-204: 10.0 wt.% CaO). The data for samples of the felsic rock suite form coherent arrays on major and trace element variation diagrams (Fig. 4), involving a negative correlation of Si with Ti, Fe, Mn, Mg, Ca, and P. Al and Na of the syenites and syenodiorites are positively correlated with Si, whereas Al and Na of the alkali granites decrease with increasing Si. Syenites and syenodiorites affected by a later alteration display higher Na_2O (7.2-10.5 wt.%) and lower K_2O (0.1-2.3 wt.%), reflected by the high modal amounts of secondary albite in these samples. Moreover these samples

partly record higher amounts of the trace elements V, 17-181 ppm (unaffected: 11-76 ppm), Zn, 32-532 ppm (unaffected: 25-201 ppm), Zr, 117-3326 ppm (unaffected: 49-2598 ppm), Nb, 52-497 ppm (unaffected: 9-178 ppm), Sr, 173-1309 ppm (unaffected: 40-674 ppm), and sums of the REE, 638-1424 ppm (unaffected: 325-399 ppm). An extremely high Sr value of 4514 ppm is recorded for the weakly altered but strongly deformed syenodiorite sample Ku-98-204, that also contains high amounts of Al_2O_3 (23.4 wt.%) and CaO (10.0 wt.%).

The trends observed for the felsic rock suite generally differ from those obtained for the anorthositic rocks. The ratio $FeO^{tot}/(MgO+FeO^{tot})$ is constantly high, ranging between 0.91-0.96 in the granite and 0.80-0.99 in the syenite/syenodiorite (except sample Sy-18 with a value of 0.71; Fig. 8a), thus plotting in the ferroan field of Frost et al. (2001). The syenites and syenodiorites are alkalic in composition, whereas the alkali granites are alkali-calcic (Fig. 8b). Most of the felsic rock samples analysed are metaluminous to slightly peraluminous Fig. 8c). They generally contain abundant LIL (Rb, Ba, REE) and HFS elements (Zr, Y, Nb), typical of A-type granites (Fig. 8d). In the discrimination diagrams Y vs. Nb and (Y+Nb) vs. Rb of Pearce et al. (1984) most samples plot in the field of within-plate granites (Fig. 8e, f). Chondrite-normalized REE plots of the felsic rock samples are almost identical (Fig. 6e). La_N/Yb_N ratios of 5.9-60.1 indicate a variable but moderate LREE enrichment. With Eu/Eu* ratios varying between 0.72 and 1.06, the rocks lack accentuated Eu anomalies. An extensive plagioclase fractionation can thus be ruled out.

The major and trace element data of the granitoid suite of NW Namibia is similar to that recorded by felsic rock suites associated with large Proterozoic anorthosite massifs like for example the adamellite suite of Harp Lake (Emslie, 1980; see Ashwal, 1993, for a review; Fig. 5).

6. U-Pb Geochronology

One weakly altered syenodiorite sample (Ku-98-201) was chosen for the U-Pb age determination on zircon. The 80 to 150 µm long zircon crystals of this syenite are slightly rounded at tips and edges and show irregular cores. The cores have weak or no cathodoluminescence (CL), whereas the margins show strong CL emission. The contrasting CL intensity suggests higher amounts of uranium and thorium in the cores (Poller et al., 2001). The zircon samples have uranium contents between 135 and 172 ppm and total Pb contents between 41 and 48 ppm. Their Th/U_{atomic}, as calculated from $(^{208}Pb/^{206}Pb)_{radiogenic}$ and the age, ranges from 0.87 to 0.93, which is typical for mafic and mantle-derived magmatic rocks (e.g., Heaman et al., 1990). Four multi-grain short-prismatic, pink to pale-brown zircon samples of igneous origin (Table 6) yield slightly discordant data that define an upper concordia intercept at 1376 ± 2 Ma (2σ, MSWD = 0.4; forced through 0 Ma; Fig. 9), which is identical with the weighted $^{207}Pb/^{206}Pb$ average age of 1376 ± 2 Ma. The low-U margins apparently had no effect on the age determination irrespective of the timing of their formation, i.e. late-magmatic or during the late hydrothermal alteration. The age of 1376 ± 2 Ma (2σ) is interpreted to date the emplacement of the felsic rock suite. It coincides with the concordant U/Pb single-zircon age of 1371 ± 2.5 Ma determined for a mangerite vein of the Angolan part of the KIC (Mayer et al., 2004) and the less precise U/Pb single-zircon age of 1385 ± 25 Ma, obtained for a leucogabbronorite sample from Namibia (Drüppel et al., 2000).

7. Isotope characteristics

7.1. Oxygen isotopic data

The utility of stable isotopes as monitors for the source rocks and processes like crustal assimilation and hydrothermal alteration of anorthosites and related rocks has been demonstrated in various studies (Taylor, 1968; Valley and O´Neill, 1982, Morrison and Valley, 1988; O´Connor and Morrison, 1999; Peck and Valley, 2000). Since both the anorthosite and the felsic rock suite are dominantly composed of feldspar, the obtained plagioclase and alkali feldspar $\delta^{18}O$ values are a good proxy for the bulk rock $\delta^{18}O$. For analyses of the oxygen isotopic composition of the anorthositic suite, plagioclase was separated from 8 samples of the dark anorthosite and 6 samples of the white anorthosite. Oxygen isotopic compositions of the felsic suite were determined for hand-picked K-feldspar and plagioclase from one quartz-syenite and 4 syenite samples. Analytical results are listed in Table 7 and shown in Fig. 10.

7.1.1. Anorthosite suite

Most plagioclase separates from rock samples of the dark anorthosite suite exhibit a narrow range in $\delta^{18}O$ (5.61-6.13 ‰), in accordance with typical values of 5.8-7.6 ‰ for magmatic anorthosite from occurrences world-wide (e.g. Ashwal, 1993). The obtained $\delta^{18}O$ values are similar to those from typical basalts and gabbros and are thus consistent with uncontaminated mantle-derived parental melts. Just one leucotroctolite sample (Ku-97-105), taken from a fault zone at the contact between the Epupa Complex and the Kunene Intrusive Complex has a considerably lower plagioclase $\delta^{18}O$ of 3.19 ‰. Extremely low $\delta^{18}O$ values of down to -6 ‰ have been reported for the Boehls Butte (Idaho) and Bitterroot (Montana) anorthosite complexes (Mora and Valley, 1988) and have been interpreted to be due to subsolidus alteration of these rocks. For the KIC, these low values could also be related to an exchange with meteoric or hydrothermal fluids. In addition, the low $\delta^{18}O$ values of the dark

anorthosite samples might be attributed to the abundance of very fine grained Fe-Ti oxide inclusions in plagioclase of these samples that might have caused a shift of the O isotope ratios to lower values.

Three of five samples of the white anorthosite display plagioclase $\delta^{18}O$ values of 5.35-6.14, i.e. in the range of unaltered plagioclase from the dark anorthosite. Thus, a pervasive alteration by circulating crustal fluids and/or meteoric water seems rather unlikely. A more convincing explanation is that the alteration of the white anorthosite results from an interaction with fluids released by younger anorthositic melts, since fluids like these would have no effects on the isotopic composition of plagioclase. This interpretation is in agreement with the preservation of the magmatic REE patterns in white anorthosite. A conspicuously high $\delta^{18}O$ value of 7.30 has been determined for plagioclase from a white anorthosite sample, which is ~ 1.4 ‰ higher than the values found in the 'normal', magmatic plagioclase of the white and dark anorthosite. This high $\delta^{18}O$ value presumably reflects contamination with crustal calc-silicate material of this rock sample. Another white anorthosite sample, taken from a major fault zone, exhibits a lower $\delta^{18}O$ value of 2.36, which agrees well with the one obtained for the fault-related leucotroctolite sample. In conclusion, the intermediate plagioclase $\delta^{18}O$ values (average: 5.88 ± 0.19 ‰ $\delta^{18}O$) of rocks from both the dark and the white anorthosite suite are interpreted to be magmatic in origin. Lower plagioclase $\delta^{18}O$ values (2.36-3.19 ‰ $\delta^{18}O$) seem to have resulted from the influx of meteoric waters restricted to faults and the higher $\delta^{18}O$ value (7.30 ‰ $\delta^{18}O$) seem to have been caused by crustal contamination.

7.1.2. Felsic rock suite

The $\delta^{18}O$ values of four alkali feldspar separates from both the syenites and syenodiorites fall in a restricted range of 7.22-7.92 ‰ (mean: 7.50 ± 0.26 ‰). Almost identical values have been obtained for plagioclase separates of the respective samples (7.20-7.52 ‰; mean: 7.36 ± 0.16 ‰), suggesting equilibrium crystallization of the two feldspars. The obtained values are interpreted to be magmatic, since the small shift of $\delta^{18}O$ values and the coincidence of the $\delta^{18}O$ values of K-feldspar and plagioclase in the felsic rocks are inconsistent with low-temperature alteration. It has to be mentioned, however, that the average $\delta^{18}O$ value of feldspar from the felsic rock suite is about 1.6 ‰ higher than the average plagioclase $\delta^{18}O$ of the anorthosites (Fig. 10). Although there is a general increase in $\delta^{18}O$ with increasing SiO_2 during closed-system crystal fractionation, since silica tends to concentrate the heavy oxygen isotope (Taylor and Sheppard, 1986), this effect is significantly smaller than the observed contrast in $\delta^{18}O$ between the felsic and anorthositic suites of the Swartbooisdrif area.

7.2. Sr and Nd isotopic data

Anorthosites and the associated felsic rocks, which locally occur as dykes within the anorthosites, show Sr(*T*) and Nd(*T*) isotopic compositions that fall into two groups, with overlapping $\varepsilon Nd_{(T)}$ values of +3.0 to –0.4 (Table 8). The $^{87}Sr/^{86}Sr_{(T)}$ values of the anorthosites define a narrow range of 0.70284 to 0.70413. This seems to be real as all samples have low $^{87}Rb/^{86}Sr$ values and high Sr contents, which resulted in only very small corrections for in situ ^{87}Sr growth (< 0.0015) and made the Sr isotopic composition little sensitive to later Sr additions. The highest $^{87}Sr/^{86}Sr_{(T)}$ values of 0.70385 and 0.70413 are recorded by the white anorthosites, which underwent both crustal contamination and later alteration. In contrast, the syenites/syenodiorites define a broader range in $^{87}Sr/^{86}Sr_{(T)}$ than the anorthosites, i.e., 0.70245

to 0.70761, whereby the relatively radiogenic $^{87}Sr/^{86}Sr_{(T)}$ values derive from samples with high Sr contents and low $^{87}Rb/^{86}Sr$ values. The highest $^{87}Sr/^{86}Sr_{(T)}$ ratios of 0.70718, 0.70761 and 0.70627 are recorded by the felsic rock samples Ku-98-201 (197 ppm Sr), Ku-98-204 (4514 ppm Sr), and Ku-98-200 (1301 ppm Sr), that underwent a variably severe secondary alteration and/or deformation. Samples with less radiogenic $^{87}Sr/^{86}Sr_{(T)}$ ratios than those of the anorthosites are characterized by both low Sr contents and relatively high $^{87}Rb/^{86}Sr$ ratios. Thus, the low $^{87}Sr/^{86}Sr_{(T)}$ values are bound to samples that are sensitive to Rb and Sr addition, which would result in a direct shift of the isotope ratios and indirectly – for $Rb_{addition} > Sr_{addition}$ – in an overcorrection of ^{87}Sr growth for the time before Rb and Sr addition. Hence, it is possible that the felsic rocks are derived from a source that had more radiogenic $^{87}Sr/^{86}Sr_{(T)}$ values than the anorthosites.

In comparison with other geochemical reservoirs present at 1.38 Ga, the Nd and Sr isotopic composition of the anorthosites and syenites have distinctly more radiogenic Nd isotopic compositions and typically less radiogenic Sr isotopic composition than the northern Namibian crust (Seth et al., 2005) and fall at the low-$^{143}Nd/^{144}Nd$ end of the field defined by sub-continental lithospheric mantle and depleted mantle (Fig. 11). Regarding their $\varepsilon Nd_{(T)}$ values of +3.0 to + 1.1, the anorthosites from the Namibian part of KIC strongly differ from two anorthosite samples of the Angolan KIC, for which distinctly lower $\varepsilon Nd_{(T)}$ values of -5.72 and -6.36 have been calculated by Slejko et al. (2002). On the other hand, the $^{87}Sr/^{86}Sr_{(T)}$ ratios of 0.7038 to 0.7045 constrained for the Angolan anorthosites by Morais et al. (1998) are in the range of the values of the Namibian samples presented in this study (i.e. 0.7028 to 0.7041).

8. Summary and conclusions

8.1. Mineralogical and geochemical characteristics of the anorthosites and related rocks

The part of the KIC exposed in NW Namibia mainly comprises pale coloured, massive, white anorthosites (i.e., anorthosites *senso stricto* and leuconorites) that are characterised by a strong deformation and alteration, i.e., sericitisation, saussuritisation, and albitisation of plagioclase and chloritization of Fe-Mg silicates. The white anorthosite massif is intruded by massive, moderately altered dark anorthositic rocks, comprising anorthosites, leucogabbronorites and leucotroctolites.

There is a small volume of associated felsic rocks, whereas gabbroic rocks are rare. Felsic rocks transecting the metapelitic rocks and orthogneisses of the Orue Unit are alkali granites and always more SiO_2-rich than the felsic rocks emplaced within the KIC, i.e., syenites and syenodiorites, suggesting that the composition of the melt parental to the felsic rock suite is modified by a veritable contamination by the respective bordering country rock. Moreover part of the felsic rock samples, especially those exposed as dykes within the KIC, show a severe late hydrothermal alteration that caused their transformation into albitites. The U-Pb zircon age of 1376 ± 2 Ma, determined for an altered syenodiorite intruding the KIC, is interpreted to date the emplacement of the felsic rock suite. It coincides with the concordant U-Pb single-zircon age of 1371 ± 2.5 Ma determined for a mangerite vein of the Angolan part of the KIC (Mayer et al., 2004) and the less precise U-Pb single-zircon age of 1385 ± 25 Ma, obtained for a leucogabbronorite sample from Namibia (Drüppel et al., 2000), suggesting that the anorthosite and the felsic rock suites are formed during the same igneous event. The age of the KIC and the respective compositions of the anorthositic and the felsic rock suites resemble that of other large Proterozoic anorthosite massifs worldwide like, for example, Harp Lake, Marcy, and Nain (see Ashwal, 1993, for a review). However, in clear contrast to

many other Proterozoic massif-type anorthosites, the KIC experienced no prograde metamorphic overprint after its emplacement at 1.38 Ga.

The early emplaced white anorthosite as well as leucogabbronorite and pyroxene-bearing anorthosite of the dark anorthosite suite generally display higher Fe/Mg ratios of the Fe-Mg silicates and higher absolute amounts of late-magmatic biotite and amphibole and of accessory apatite when compared to the olivine-bearing anorthosites and leucotroctolites of the dark anorthosite suite. Moreover, both units frequently display crustal xenoliths of calc-silicate material. The highest Sr concentrations have been obtained for the white anorthosite and the pyroxene-bearing anorthosite/leucogabbronorite of the dark anorthosite suite, which, at the same time, exhibit the highest overall trace element abundances. Lowest average Sr concentrations (470-640 ppm) are recorded for the olivine-bearing anorthosites and leucotroctolites, corresponding with the highest average An-contents of plagioclase and lowest total sums of incompatible trace elements. An inverse correlation between Sr and the An-content is a common feature of layered intrusions and is generally attributed to plagioclase fractionation, causing a decrease of the Sr content in the melt (see Ashwal, 1993, for a review). On the other hand it has been demonstrated by Duchesne (1978) for the layered Bjerkrem-Sogndal bodies of Norway that plagioclase fractionation may cause an increase of Sr in the melt. In the case of the KIC, however, this trend is more likely caused by contrasting contamination with calc-silicate crustal material. Younger anorthosite melts may have used already existing pathways through the crust provided by the previously intruded anorthositic magma, i.e., ascending mainly through anorthositic country rock. In case of the white anorthosite, however, the trace element patterns may additionally be obscured by later secondary processes like the severe hydrothermal alteration and deformation recorded by most samples.

8.2. Origin of the anorthositic and felsic rock suites

The respective mineral compositions of the granite-syenite suite appear to extend the compositional range of the anorthositic rocks towards higher Fe/Mg ratios and lower Al of the Fe-Mg silicates (pyroxene, amphibole, epidote and chlorite) and lower An contents of plagioclase. The relative changes in the mineral compositions could provide evidence for consanguinity between the two rock suites. However, intermediate mineral compositions, bridging the gap between those of the anorthositic and the felsic rock suite, are missing. Like the Harp Lake massif, Labrador, the Namibian felsic and anorthositic rock suites are characterized by chemical discontinuities, reflecting the lack of rock types of intermediate chemical composition (Fig. 5), which is a common feature of unmetamorphosed anorthosite massifs (Ashwal, 1993). The difference in the magmatic $\delta^{18}O$ values of feldspar from granitoids and anorthositic rocks also supports a non-comagmatic relationship of the two suites. The rather homogeneous but high $\delta^{18}O$ values of feldspar from the felsic rock suite (7.36 ± 0.16 ‰) when compared to those of the anorthositic rock suite (5.88 ± 0.19 ‰ $\delta^{18}O$) point to a crustal source for the felsic suite. On the other hand, the values obtained for plagioclase of the anorthosite suites are consistent with uncontaminated mantle-derived parental melts. The contrast in $^{87}Sr/^{86}Sr_{(T)}$ ratios between anorthositic (0.7028-0.7041) and the felsic rock suites (0.7025-0.7076) also suggest a different source of the two units, in line with $\delta^{18}O$ values. If the variable Sr, Nd, and O isotopic signatures of both the anorthositic and felsic rocks are due to the assimilation of crustal material, the isotopic composition of Sr and O were more affected than the isotopic composition of Nd. Such a Sr-Nd-O decoupling indicates that the assimilated rocks should have had relatively high Sr contents, but low Nd contents, which is typically found for marine carbonates, but not in silicic crustal material. Assimilation of carbonates is a particularly attractive explanation as there locally occur

abundant xenoliths of crustal calc-silicate material and carbonate assimilation not only accounts for the elevated $^{87}Sr/^{86}Sr$, but also for the heavy $\delta^{18}O$ values. In case of the felsic rocks this trend is rather caused by the late hydrothermal alteration of these rocks. In conclusion, our dataset demonstrates that the anorthositic lithologies and the felsic rock suite represent two chemically independent suites. The source of the anorthositic rocks is a mantle-derived liquid that, during their uprise, was modified by minor crustal contamination. Hereby crustal contamination, as evident from the abundance of crustal xenoliths, low Ca/(Ca+Na) ratios, and high amounts of late-magmatic biotite, amphibole and apatite, is predominantly displayed by the early emplaced white anorthosite and the leucogabbronorite of the dark anorthosite suite. In contrast, leucotroctolites and olivine anorthosites are characterized by high An-contents of plagioclase and a mostly unhydrous mineralogy; late-magmatic biotite and amphibole are rare. Melts parental to the felsic rocks presumably originate by anatexis of the lower crust or at least experienced a stronger crustal contamination than the anorthosites, either in the magma chamber or during their ascent. Granite bodies emplaced in the Epupa Complex were additionally affected by contamination of the granitic magma with metasedimentary and metavolcanic crustal material during their uprise.

The εNd values of the anorthositic rocks, calculated back to their emplacement age of 1385 Ma given by U-Pb zircon data (Drüppel et al., 2000), range between 1.1 and 3.0, indicating a time-integrated weakly depleted character of the parental magma with respect to CHUR. Corresponding Nd model ages of 2.01-1.61 Ga, calculated with respect to a depleted mantle curve, are significantly older than the crystallization age of the anorthosites. Model ages older than the intrusion ages have also been reported for several anorthosite massifs and are either ascribed to crustal contamination effects (e.g. Ashwal, 1993; Ashwal et al., 1998), in which case the model ages lack geological significance (cf. Arndt & Goldstein, 1987), or to a lower crustal origin of the anorthosites (e.g. Schiellerup et al., 2000; Wiszniewska et al.,

2002). The hypothesis that anorthosites originate in the lower crust has found increasing support in recent years (Taylor et al., 1984; Duchesne et al., 1999; Longhi et al., 1999; Schiellerup et al., 2000; Selbekk et al., 2000, Wiszniewska et al., 2002), based on Re-Os isotope data and experimental investigations. In case of the KIC, the geochemical characteristics as well as O, Sr, and Nd isotope data indicate a mantle origin of the anorthosites and hence suggest that the magma parental to the anorthosites formed by partial melting of the upper mantle. The same signatures, however, may have been preserved also during lower crustal melting of a previously emplaced mantle-derived mafic rock under dry conditions. Indeed, igneous protolith ages of 2.0-1.7 Ga, calculated for granulite and amphibolite facies mafic rocks of the Epupa Complex (Seth et al., 2005), would fit in this model, suggesting the following tectono-metamorphic scenario: Emplacement of a large mafic bodies at ca. 2.0-1.7 Ga, subsequent granulite facies metamorphism of the mafic rocks metamorphism at 1.52 Ga and finally partial melting with formation of the anorthositic magma at 1.38 Ga. A scenario like this has been invoked by Schiellerup et al. (2000) for the Rogaland anorthosites, Norway, and by Wiszniewska et al. (2002) for the Mazury complex, Poland. In case of the KIC, however, this alternative model seems rather unlikely. With an estimated surface area of ca. 18.000 km^2 the KIC has an enormous size when compared to the anorthosites from Norway and Poland. Moreover the KIC is characterized by an extraordinary compositional and textural homogeneity, being almost entirely composed of anorthosite, leucogabbronorite, and leucotroctolite with high-Ca plagioclase, whereas related gabbroic or felsic lithologies are rare. If the anorthositic magmas of the KIC originated by partial melting of a lower continental mafic crust or foundered mafic plutons, these mafic source regions must be of unrealistically large and homogeneous in composition. Moreover, the production of such large volumes of anorthositic magma by partial melting would presumably lead to a gravitational collapse of the lower crustal source regions. Therefore, we interpret the parental

magma of the anorthosites of the Kunene Intrusive Complex to be derived from partial melting of the upper mantle with anatexis of crustal material leading to the formation of the associated felsic rocks.

8.3. Comparison to other parts of the Kunene Intrusive Complex

Due to difficult access during the civil war, most studies of the northern part of the KIC are based on old field data and sampling (Carvalho & Alves, 1990, 1993; Silva, 1990, 1992). Recent detailed field work in combination with petrographical investigations is lacking for most of the Angolan part of the KIC, except restricted areas around Lufinda, Dongue and Chiange in Angola (Ashwal & Twist, 1994; Morais et al., 1998; Slejko et al., 2002; Mayer et al., 2004; Fig. 1). Based on satellite imagery Ashwal & Twist (1994) suggested that the KIC represents a composite massif-type anorthosite, composed of at least eight distinct anorthosite bodies with probably individual petrogenetic evolution.

Regarding their geochemical composition the Namibian rock suite is characterised by a similar variability of geochemical compositions and higher average amounts of Na_2O when compared to the anorthosites from the Angolan part of the KIC (Silva, 1990, 1992; Morais et al., 1998; Fig. 12). Based on the mineral chemistry data and isotope characteristics of the anorthosites from Angola a northern (average An-content of plagioclase: 70 ± 5 mol.%; $^{87}Sr/^{86}Sr_{(T)}$: 0.7038; εNd: -5.72) and a southern zone (average An-content of plagioclase: 53 ± 5 mol.%; $^{87}Sr/^{86}Sr_{(T)}$: 0.7045; εNd: -6.36) have been distinguished, that are separated by a belt of granitoid intrusions (Morais et al., 1998; Slejko et al., 2002). Likewise the Namibian KIC can be subdivided into two units, the white anorthosite (An-content of plagioclase: 43-53 mol.%; $^{87}Sr/^{86}Sr_{(T)}$: 0.7039-0.70413; εNd: 1.1-2.0) and the dark anorthosite massif (An-content of plagioclase: 43-75 mol.%; $^{87}Sr/^{86}Sr_{(T)}$: 0.7028-0.7036; εNd: 1.7-3.0). Both rock

units presumably represent individual anorthosite intrusions that underwent a distinct petrogenetic evolution. These are marked by a contrasting contamination with crustal material and also strongly differ from the two anorthosite bodies identified in Angola.

The petrographical features of the Namibian leucotroctolite, leucogabbronorite, and anorthosite samples of the dark anorthosite suite investigated in this study resemble those reported for the northern, Angolan, part of the KIC (Silva, 1990, 1992; Ashwal & Twist, 1994; Morais et al., 1998; Slejko et al., 2002). However, subsolidus reaction textures like garnet-bearing corona structures of the dark anorthosites from NW Namibia (Drüppel et al., 2001) have not yet been observed. In the Lufinda-Dongue area, the presence of cogenetic dolerites and mangerites is interpreted in favour of a shallow emplacement level of the anorthosite (Morais et al., 1998; Slejko et al., 2002). Pressures of 3-5 kbar have been estimated by Slejko et al. (2002) for the subsolidus re-equilibration of orthopyroxene-clinopyroxene pairs. In contrast, distinctly higher pressures of 7.3 ± 0.9 kbar and of 6.5 ± 0.6 kbar were constrained for the subsolidus formation of garnet-bearing corona structures in the Namibian leucotroctolites (Drüppel et al., 2001; Drüppel, 2003) and the magmatic crystallization of hastingsite in the associated felsic rocks (Drüppel, 2003), respectively. Similar pressures of 6.5 ± 0.6 kbar were constrained for a contact-metamorphic hornfels of the Orue Unit by Brandt (2003). As is evident from Fig. 1, however, the Angolan and Namibian study areas are at least 150 km apart from each other and detailed field work as well as mineralogical investigations of the anorthosites in the intermediate southern Angolan part of the KIC are lacking so far. Future investigations will help to decide whether the apparent differences in the erosion level of ca. 9 km is due to a continuous gradient in exposed crustal depth or due to offsets by deep fracture zones as for example the Serpa-Pinto lineament or the Kunene River fault.

The emplacement of the KIC and the associated granitic rocks at the southern margin of the Congo Craton marks the beginning of widespread Mesoproterozoic igneous activity in southern Africa. The Mesoproterozoic KIC is possibly related to the Mesoproterozoic Kibaran Belt of the Democratic Republic of Congo and Tanzania, that is characterised by voluminous Mesoproterozoic mafic and A-type granite magmatism at 1383-1371 Ma (Tack et al., 2002; see Johnson et al., 2005, for a review). This age interval resembles that constrained for the anorthosites of the KIC and related rocks, however, intermediate zones between the KIC and the Kibaran belt are not exposed. If the KIC and the Kibaran belt were related in the Mesoproterozoic, they might have been part of a major northeast striking extensional belt that formed during the early stages of separation of the Congo and the southern Kapvaal-Zimbabwe cratons. On the other hand, the KIC may also represent a postorogenic pluton, with the mantle and crustal melts being formed by lithospheric delamination (Black and Liégeois, 1993) during a post-orogenic collapse that followed widespread Palaeoproterozoic orogenic activity in central and southern Africa at 2.2-1.6 Ga, the so-called Eburnian Orogeny (e.g. Cahen et al., 1984; Carvalho et al., 2000).

Acknowledgements

We are grateful to Jochen Hoefs (University of Göttingen) for providing the O-isotope analyses. We also wish to thank Uli Schüssler (University of Würzburg) as well as Dieter Rhede and Oona Appelt (GFZ Potsdam) for their advice and help with the EMP work, Sönke Brandt (University of Kiel) for providing helpful information regarding the evolution of the metamorphic Epupa Complex, and Philipp Gleißner (Technical University of Berlin) for stimulating discussions during the 2006 field season. The manuscript benefited from the comments of two anonymous reviewers. Thanks are also due to Peter Späthe (University of

Würzburg) and to Gerhard Berger (GFZ Potsdam) for thorough preparation of the thin sections and polished sections. Our work was sponsored by the Deutsche Forschungsgemeinschaft (grant DR 744/1-1), which is gratefully acknowledged.

References

Anderson, J.L., 1980. Mineral equilibria and crystallization conditions in the late Precambrian Wolf River rapakivi massif, Wisconsin. Am. J. Sci. 280, 289-332.

Anderson, J.L., Bander, E.E., 1989. Nature and origin of Proterozoic A-type granitic magmatism in the southwestern United States of America. Lithos 23, 19-52.

Arndt, N.T., Goldstein, S.L., 1987. Use and abuse of crust-formation ages. Geology 15, 893-895.

Ashwal, L.D., 1993. Anorthosites. Minerals and Rocks Series 21. Springer-Verlag, Berlin.

Ashwal, L.D., Hamilton, M.A., Morel, V.P.I., Rambeloson, R.A., 1998. Geology, petrology and isotope geochemistry of massif-type anorthosites from southwest Madagascar. Contrib. Miner. Petrol. 133, 389-401.

Ashwal, L.D., Twist, D., 1994. The Kunene complex, Angola/Namibia: a composite massif-type anorthosite complex. Geol. Mag. 131, 579-591.

Black, R, Liégeois, J., 1993. Cratons, mobile belts, alkaline rocks and continental lithospheric mantle: the Pan-African testimony. Journal of the Geological Society 150, 89-98.

Borthwick, J., Harmon, R.S., 1982. A note regarding ClF3 as an alternative to BrF5 for oxygen isotope analysis. Geochim. Cosmoch. Acta 46, 1665-1668.

Brandt, S., 2003. Metamorphic evolution of ultrahigh-temperature granulite facies and upper amphibolite facies rocks of the Epupa Complex, NW Namibia. Dr. rer. nat. thesis, University of Würzburg

Brandt, S., Klemd, R., Okrusch, M., 2003. Ultrahigh-temperature metamorphism and multistage evolution of garnet-orthopyroxene granulites from the Proterozoic Epupa Complex, NW Namibia. J. Petrol. 44, 1121-1144.

Brandt, S., Will, T.M., Klemd, R., 2007. Ultrahigh-temperature metamorphism and anticlockwise PT paths of sapphirine-bearing orthopyroxene-sillimanite gneisses from the Proterozoic Epupa Complex, NW Namibia. Precambr. Res. (in press).

Cahen, L., Snelling, N.J., Delhal, J., Vail, J.R., Bonhomme, M., Ledent, D., 1984. The Geochronology and evolution of Africa. Oxford University Press, Oxford.

Carvalho, H. de, Alves, P., 1990. Gabbro-Anorthosite Complex of SW Angola/ NW Namibia. Inst. Inv. Cientifica Tropical, Série de Ciências da Terra, Communicações 2, 1-66.

Carvalho, H. de, Alves, P., 1993. The Precambrian of SW Angola and NW Namibia. Garcia de Orta, Série de Ciências da Terra, Communicações 4, 1-38.

Carvalho, H. de, Tassinari, C., Alves, P.H., Guimarães, F., Simões, M.C., 2000. Geochronological review of the Precambrian in western Angola: links with Brazil. J. Afr. Earth Sci. 31, 383-402.

de Waard, D., 1970. The anorthosite-charnockite suite of rocks of Roaring Brook Valley in the eastern Adirondacks (Marcy Massif). Am. Miner. 55, 2063-2075.

Cox, K.G., Bell, J.D., Pankhurst, R.J., 1979. The interpretation of igneous rocks. George Allen & Unwin Ltd, London.

Drüppel, K., 1999. Petrologie und Geochemie von Anorthositen des Kunene-Intrusiv-Komplexes, NW Namibia. Diploma thesis, University of Würzburg.

Drüppel, K., 2003. Petrogenesis of the Mesoproterozoic anorthosite, syenite and carbonatite suites of NW Namibia and their contribution to the metasomatic formation of the Swartbooisdrif sodalite deposits. Dr. rer. nat. thesis, University of Würzburg.

Drüppel, K., Littmann, S., Okrusch, M., 2000. Geo- und isotopenchemische Untersuchungen der Anorthosite des Kunene-Intrusiv-Komplexes (KIC) in NW-Namibia. Berichte der Deutschen Mineralogischen Gesellschaft, Beiheft zum Eur. J. Miner. 12, 37.

Drüppel, K., Hoefs, J., Okrusch, M., 2005. Fenitizing processes induced by ferrocarbonatite magmatism at Swartbooisdrif, NW Namibia. J. Petrol. 46, 377-406.

Drüppel, K., von Seckendorff, V., Okrusch, M., 2001. Subsolidus reaction textures in anorthosites of the Kunene Intrusive Complex, NW Namibia. Eur. J. Miner. 13, 289-309.

Duchesne, J.-C., 1978. Quantitative modelling of Sr, Ca, Rb and K in the Bjerkrem-Sogndal layered lopolith (S.W. Norway). Contrib. Miner. Petrol. 66, 175-184.

Duchesne, J.-C., 1984. Massif anorthosites: another partisan review. In: Brown W.L. (Ed.), Feldspars and feldspathoids. Reidel, Dordrecht, 411-433.

Duchesne, J.C., Liégeois, J.P., Vander Auwera, J., Longhi, J., 1999. The crustal tongue melting model and the origin of massive anorthosites. Terra Nova 11, 100-105.

Dulski, P., 1994. Interferences of oxide, hydroxide and chloride analyte species in the determination of rare earth elements in geological samples by inductively coupled plasma-mass spectrometry. Fresenius J. Analytical Chemistry 350,194-203.

Emslie, R.F., 1980. Geology and petrology of the Harp Lake Complex, Central Labrador: an example of Elsonian magmatism. Geological Survey of Canada Bulletin 293, 1-136.

Emslie, R.F., 1985. Proterozoic anorthosite massifs. In: Tobi, A., Touret, J.L.R. (Eds.), The Deep Proterozoic Crust in the North Atlantic provinces. NATO ASI Series C 158, Reidel, Dordrecht, 39-60.

Emslie, R.F., 1991. Granitoids of rapakivi granite-anorthosite and related associations. Precambr. Res. 51, 173-192.

Emslie, R.F., Hamilton, M.A., Therault, R.J., 1994. Petrogenesis of mid-Proterozoic anorthosite-mangerite-charnockite-granite, AMCG complex: isotopic and chemical evidence from the Nain Plutonic Suite. J. Geol. 102, 539-558.

Frost, B.R, Barnes, C.G., Collins, W.J., Arculus, R.J., Ellis, D.J., Frost, C.D., 2001. A geochemical classification for granitic rocks. J. Petrol. 42, 2033-2048.

Fuhrmann, M.L., Frost, B.R., Lindsley, D.H., 1988. Crystallization conditions of the Sybille Monzosyenite, Laramie Anorthosite Complex, Wyoming. J. Petrol. 29, 699-729.

Gerstenberger, H., Haase, G., 1997. A highly effective emitter substance for mass spectrometric Pb isotope ratio determinations. Chem. Geol. 136, 309–312.

Heaman, L.M., Bowins, R., Crocket, J., 1990. The chemical composition of igneous zircon suites: Implications for geochemical tracer studies. Geochim. Cosmoch. Acta 55, 1597-1607.

Jacobsen, S.B., Wasserburg, G.J., 1979. Nd and Sr isotopic study of the Bay of Islands ophiolite complex and the evolution of the source of midocean ridge basalts. J. Geophys. Res. 84, 7429-7445.

Jaffey, A.H., Flynn, K.F., Glendenin, L.E., Bentley, W.C., Essling, A.M., 1971. Precision measurement of half-lives and specific activities of ^{235}U and ^{238}U. Physics Reviews C4, 1889–1906.

Johnson, S.P., Rivers, T., De Waele, B., 2005. A review of the Mesoproterozoic to early Palaeozoic magmatic and tectonothermal history of south-central Africa: implications for Rodinia and Gondwana. J. Geol. Soc. London 162, 433-450.

Köstlin, E.C., 1967. The geology of part of the Kunene basic complex, Kaokoveld, South West Africa. M.Sc. Thesis, University of Cape Town.

Köstlin, E.C., 1974. The Kunene basic complex, northern South West Africa. In: Kröner, A. (Ed.), Contributions to the Precambrian geology of southern Africa. University of Cape Town Bulletin 15, Capetown, 123-135.

Krogh, T.E., 1973. A low contamination method for hydrothermal decomposition of zircon and extraction of U and Pb for isotopic age determinations. Geochim. Cosmoch. Acta 37, 485-494.

Littmann, S., Romer, R.L., Okrusch, M., 2000. Nephelinsyenite der Epembe-Swartbooisdrif-Alkali-Provinz (ESAP)/ NW Namibia. Berichte der deutschen Mineralogischen Gesellschaft, Beihefte zum Eur. J. Miner. 12: 115.

Longhi, J., Ashwal, L.D., 1985. Two-stage models for lunar and terrestrial anorthosites: Petrogenesis without a magma ocean. J. Geophys. Res. 90, C571-C584.

Longhi, J., Vander Auwera, J., Fram, M.S., Duchesse, J.-C., 1999. Some Phase Equilibrium Constraints on the Origin of Proterozoic (Massif) Anorthosites and Related Rocks. J. Petrol. 40, 339-362.

Mayer, A., Sinigoi, S., Miguel, L.G., Morais, E., Petrini, R., 2000. Kibaran ages in the Kunene anorthositic complex. GEOLUANDA 2000, Abstract volume, 106.

Mayer, A., Hofmann, A.W., Sinigoi, S., Morais, E., 2004. Mesoproterozoic Sm–Nd and U–Pb ages for the Kunene Anorthosite Complex of SW Angola. Precambr. Res. 133, 187-206.

Menge, G.F.W., 1996. The eastern portion of the Kunene complex, its satellite intrusions and the alkaline suite between Epembe and Swartbooisdrif. Unpublished Report, Univerity of Cape Town.

Menge, G.F.W., 1998. The antiformal structure and general aspects of the Kunene Complex. Z. Dt. Geol. Ges. 149, 431-448.

Mitchell J.N., Scoates J.S., Frost C.D., 1995. High-Al gabbros in the Laramie anorthosite complex, Wyoming: implications for the composition of melts parental to Proterozoic anorthosites. Contrib. Miner. Petrol. 119, 166-180.

Mora, C.I., Valley, J.W., 1988. Channelized meteoric-hydrothermal alteration of the Boehls Butte and Bitterroot anorthosites, northern ID and MT. Eos 69, 1489.

Morais, E., Sinigoi, S., Mayer, A., Mucana, A., Miguel, L.G., Rufino Neto, J., 1998. The Kunene gabbro-anorthosite Complex: preliminary results based on new field and chemical data. Afr. Geosci. Rev. 5, 485-498.

Morimoto, N., 1988. Nomenclature of pyroxenes. Miner. Mag. 52, 535-550.

Morrison, J., Valley, J.W., 1988. Contamination of the Marcy anorthosite massif, Adirondack Mountains, NY: petrologic and isotopic evidence. Contrib. Miner. Petrol. 98, 97-108.

O´Connor, Y.-L., Morrison, J., 1999. Oxygen isotope constraints on the petrogenesis of the Sybille intrusion of the Proterozoic Laramie anorthosite complex. Contrib. Miner. Petrol. 136, 81-91.

Pearce, J.A., Harris, N.B.W., Tindle, A.G., 1984. Trace element discrimination diagrams for the tectonic interpretation of granitic rocks. J. Petrol. 25, 956-983.

Pearce, N.J.G., Perkins, W.T., Westgate, J.A., Gorton, M.P., Jackson, S.E., Neal, C.R., Chenery, S.P., 1997. A compilation of new and published major and trace element data for NIST SRM 610 and NIST SRM 612 glass reference materials. Geostandards Newsletter 21, 115-144.

Peck, W.H., Valley, J.W., 2000. Large crustal input into high δ18O anorthosite massifs of the southern Grenville Province: new evidence from the Morin Complex, Quebec. Contrib. Miner. Petrol. 139, 402-417.

Plessen, H.-G., 1997. Analytik und Geochemie der Platingruppenelemente in magmatischen Gesteinen. Dr. rer. nat. thesis, University of Potsdam.

Poller, U., Uher, P., Janák, M., Plasienka, D., 2001. Late Cretaceous age of the Rochovce granite, Western Carpathians, constrained by U/Pb single-zircon dating in combination with cathodoluminescence imaging. Geologica Carpathica 52, 41-47.

Romer, R.L., Heinrich, W., Schröder-Smeibidl, B., Meixner, A., Fischer, C.-O., Schulz, C., 2005. Elemental dispersion and stable isotope fractionation during reactive fluid-flow and fluid immiscibility in the Bufa del Diente aureole, NE-Mexico: Evidence from radiographies and Li, B, Sr, Nd, and Pb isotope systematics. Contrib. Miner. Petrol. 149, 400-429.

Schiellerup, H., Lambert, D., Presvik, T., Robins, B., McBride, J.S., Lars, R.B., 2000. Re–Os isotopic evidence for a lower crustal origin of massif-type anorthosites. Nature 405, 781-784.

Seifert, K.E., 1978. Anorthosite-mangerite relations on Barker Mountain, New York. Geol. Soc. Am. Bull. 89, 245-250.

Selbekk, R.S., Skjerlie, K.P., Pedersen, R.B., 2000. Generation of anorthositic magma by H_2O-fluxed anatexis of silica-undersaturated gabbro: An example from the north Norwegian Caledonides. Geol. Mag. 137, 609–621.

Seth, B., Armstrong, R.A., Brandt, S., Villa, I.M., Kramers, J.D., 2003. Mesoproterozoic U-Pb and Pb-Pb ages of granulites in NW Namibia: reconstructing a complete orogenic cycle. Precambr. Res. 126, 147-168.

Seth, B., Armstrong, R.A., Büttner, A., Villa, I.M., 2005. Time constraints for Mesoproterozoic upper amphibolite facies metamorphism in NW Namibia: a multi-isotopic approach. Earth Plan. Sci. Lett. 230, 355-378.

Silva, Z.C.G., 1990. Geochemistry of the gabbro-anorthosite Complex of Angola. J. Afr. Earth Sci. 10, 683-692.

Silva, Z.C.G., 1992. Mineralogy and cryptic layering of the Kunene anorthosite complex of SW Angola and Namibia. Miner. Mag. 56, 319-327.

Slejko, F.F., Demarchi, G., Morais, E., 2002. Mineral chemistry and Nd isotopic composition of two anorthositic rocks from the Kunene complex (South western Angola. J. Afr. Earth Sci. 35, 77-88.

Steiger, R.H., Jäger, E., 1977. Subcommission on geochronology: Convention on the use of decay constants in geo- and cosmochronology. Earth Plan. Sci. Lett. 36, 359-362.

Streckeisen, A., 1974. How should charnockitic rocks be named? In: Bellière, J., Duchesne, J.C. (Eds.), Géologie des Domaines Cristallins. Sociéte Géologique de Belgique, Centenary volume, Liège, 349-360.

Tack, L., Fernandez-Alonso, M., Tahon, M., Wingate, M.T.D., Barritt, S., 2002. The `northeastern Kibaran belt´ (NKB) and its mineralisations reconsidered: new constraints from a revised lithostratigraphy, a GIS-compilation of existing geological maps and a review of recently published as well as unpublished igneous emplacement ages in Burundi. Abstracts, 11th IAGOD Quadrennial Symposium and Geocongress, Windhoek, 6.

Taylor, H.P., 1968. Oxygen isotope studies of anorthosites, with particular reference to the origin of bodies in the Adirondack Mountains, New York. In: Isachsen, Y.W. (ed.) Origin of anorthosite and related rocks. N.Y. State Museum and Science Service Memoir 18, 111-134.

Taylor, S.R., Campbell, I.H., McCulloch, M.T., McLennan S.M., 1984. A lower crustal origin for massif-type anorthosites. Nature 311, 372-374.

Taylor, H.P., Sheppard, S.M.F., 1986. Igneous rocks I. Processes of isotopic fractionation and isotope systematics. In: Valley, J.W., Taylor, H.P., O´Neil, J. (Eds.), Stable isotopes in high temperature geological processes. Mineralogical Society of America, Chelsea, Michigan, 227-269.

Tegtmeyer, A., Kröner, A., 1985. U-Pb zircon ages for granitoid gneisses in northern Namibia and their significance for Proterozoic crustal evolution of Southwestern Africa. Precambr. Res. 28, 311-326.

Torquato, J.R., Silva, A.T.S.F. da, Cordani, U.G., Kawashita, K., 1979. A evolução geológica do Cinturão Móvel do Quipungo no Ocidente de Angola. Anais Academia Brasileira Ciências 51, 133-143.

Valley, J.W., O´Neil, J.R., 1982. Oxygen isotope evidence for shallow emplacement of Adirondack anorthosite. Nature 300, 497-500.

Von Seckendorff, V., Drüppel, K., Okrusch, M., Littmann, S., Cook, N., 2000. Oxide-sulphide relationships in sodalite-bearing metasomatites of the Epembe-Swartbooisdrif Alkaline Province, North-West Namibia. Mineralium Deposita 35, 430-450.

Whalen, J.B., Currie, K.L., Chappell, B.W., 1987. A-type granites: geochemical characteristics, discrimination and petrogenesis. Contrib. Miner. Petrol. 95, 407-419.

Wiebe, R.A., 1994. Proterozoic anorthosite complexes. In: Condie, K.C. (Ed.), Proterozoic crustal Evolution. Elsevier, Amsterdam, 215-261.

Wilson, M., 1989. Igneous petrogenesis – a global tectonic approach. Harper Collins Academic, London.

Wiszniewska, J., Claesson, S., Stein, H.J., Vander Auwera, J., Duchesne, J.–C., 2002. The north-eastern Polish anorthosite massifs: petrological eochemical and isotopic evidence for a crustal derivation. Terra Nova 14, 451-460.

Zuleger, E., Erzinger, J., 1988. Determination of the REE and Y in silicate materials with ICP-AES. Fresenius Z. Analytische Chemie 332, 140-143.

FIGURE CAPTIONS

Fig. 1. Geologic overview map of the Kunene Intrusive Complex in SW Angola and NW Namibia. Map simplified and modified after Carvalho & Alves (1990). Outlined areas mark regions of detailed mapping in the Angolan part (Ashwal & Twist, 1994; Morais et al., 1998; Slejko et al., 2002; Mayer et al., 2004) and in the Namibian part of the KIC (Menge, 1998; Drüppel et al., 2001; Drüppel, 2003).

Fig. 2. Geologic overview map of the southern Kunene Intrusive Complex in NW Namibia. Map modified after Menge (1998) based on new field data and satellite images. Locations for geochemical analyses and age determinations are marked.

Fig. 3. Polished-section photomicrographs of the anorthositic rocks of the KIC (a, b) and the related felsic rocks (c, d). Plane-polarized light (a). Cross-polarized light (b-d). (a) Subhedral, interstitial olivine is surrounded by irregular rims of orthopyroxene and late amphibole and biotite that fill the open spaces between plagioclase crystals. (b) Interstices between coarse-grained, anhedral cumulus plagioclase are filled by interstitial olivine that is surrounded by broad clinopyroxene rims. (c) Subhedral, tabular plagioclase displays straight grain boundaries against microperthitic K-feldspar. (d) Euhedral clinopyroxene inclusion in plagioclase. (*Am* amphibole, *Bt* biotite, *Kfs* K-feldspar, *Ol* olivine, *Opx* orthopyroxene, *Pl* plagioclase).

Fig. 4. Variations of selected major and trace element contents of the anorthositic rocks of the KIC and the related felsic rocks.

Fig. 5. Compositional variability of both the anorthositic and the felsic rock suite compared to similar lithologies of the Harp Lake massif, Labrador (stippled boundaries; Emslie, 1980). Same symbols as Fig. 4. (a) Plot of molar $Fe^{tot}/(Fe^{tot}+Mg)$ vs. SiO_2 and (b) Na_2O+K_2O vs. SiO_2. (*S* syenite, *SD* syenodiorite).

Fig. 6. Diagrams showing the variations in chondrite-normalized rare earth element abundances for the anorthositic rocks of the KIC and the associated felsic rock suite (normalisation factors after Pearce et al., 1997).

Fig. 7. Composition of the felsic rock suite expressed in the $Na_2O + K_2O$ vs. SiO_2 classification diagram for plutonic rocks after Cox et al. (1979).

Fig. 8. Compositional characteristics of the felsic rock suite expressed in various binary discrimination diagrams. (a) Plot of $FeO^{tot}/(FeO^{tot}+MgO)$ vs. SiO_2 with the boundary between ferroan and magnesian fields given by Frost et al. (2001). (b) Plot of the modified alkali-lime index Na_2O+K_2O-CaO vs. SiO_2 (Frost et al., 2001). (c) Shand´s alkalinity index (plot of $Al_2O_3/(Na_2O+K_2O)_{molar}$ vs. $Al_2O_3/(Na_2O+K_2O+CaO)_{molar}$). (d) A-type granitoid discrimination diagram after Whalen et al. (1987). (e) and (f) Tectonic environment discrimination diagrams after Pearce et al. (1984). (*ORG* orogenic granite, *syn-COLG* syn-collisional granite; *VAG* volcanic arc granite, *WPG* within-plate granite).

Fig. 9. Isochron $^{206}Pb/^{204}Pb$ vs $^{208}Pb/^{204}Pb$ diagram for zircon samples of syenodiorite Ku-98-201, Swartbooisdrif, Namibia (data from Table 6)

Fig. 10. Plot of $\delta^{18}O$ vs. SiO_2 for the anorthositic rocks of the KIC and the felsic rock suite (see text for discussion).

Fig. 11. Initial Sr-Nd isotope systematics of c. 1.38 Ga anorthosites and related felsic rocks in comparision with depleted mantle (light grey shaded area) and Palaeoproterozoic crust of northern Namibia (dark grey shaded area). Note the sub-horizontal arrangement of the anorthosite and fesic rock samples. The Sr and Nd isotopic composition of the crust was estimated from 1.9 Ga orthogneisses (Seth et al., 2005) recalculated to 1.38 Ga. The composition of the mantle reservoirs was estimated, assuming Rb/Sr and Sm/Nd typical for these reservoirs (e.g., Wilson, 1989).

Fig. 12. Diagram of MgO vs. $CaO/(CaO+Na_2O)$ for available geochemical data on the Kunene Complex. (a) Geochemical composition of the white and dark anorthosite suites from NW Namibia. (b) Geochemical composition of anorthositic rocks from Angola (Silva, 1992 and Morais et al., 1998).

TABLE CAPTIONS

Table 1a Representative electron microprobe analyses of plagioclase of the anorthosite suite. Table 1b Representative electron microprobe analyses of feldspar of the felsic rock suite.

Table 2 Representative electron microprobe analyses of pyroxene of the anorthosite and the felsic rock suites.

Table 3 Representative electron microprobe analyses of amphibole of the anorthosite and the felsic rock suites.

Table 4 Selected major and trace element data of the anorthosite and the felsic rock suites.

Table 5 Rare earth element data of the anorthosite and the felsic rock suites.

Table 6 U-Pb analytical results for zircon from the syenodiorite sample Ku-98-201, Swartbooisdrif, Namibia.

Table 7 Oxygen isotopic data of feldspar of the anorthosite and the felsic rock suites.

Table 8 Sr and Nd isotope data for anorthosites and felsic rocks from NW Namibia.

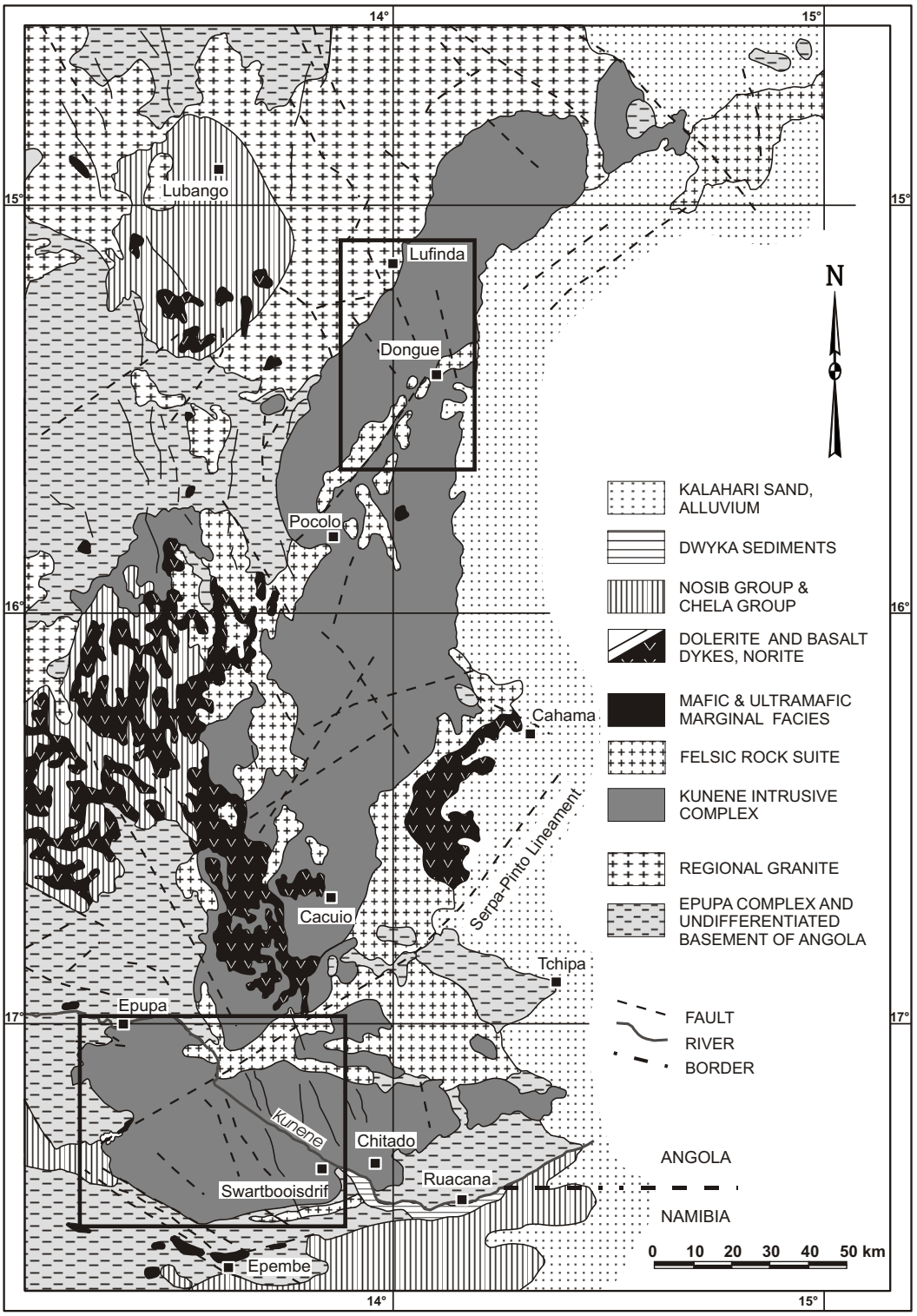
14°
15°
16°
17°
Lubango
Lufinda
Dongue
Pocolo
Cahama
Cacuio
Tchipa
Epupa
Kunene
Chitado
Swartbooisdrif
Ruacana
Epembe
Serpa-Pinto Lineament
N
KALAHARI SAND, ALLUVIUM
DWYKA SEDIMENTS
NOSIB GROUP & CHELA GROUP
DOLERITE AND BASALT DYKES, NORITE
MAFIC & ULTRAMAFIC MARGINAL FACIES
FELSIC ROCK SUITE
KUNENE INTRUSIVE COMPLEX
REGIONAL GRANITE
EPUPA COMPLEX AND UNDIFFERENTIATED BASEMENT OF ANGOLA
FAULT
RIVER
BORDER
ANGOLA
NAMIBIA
0 10 20 30 40 50 km

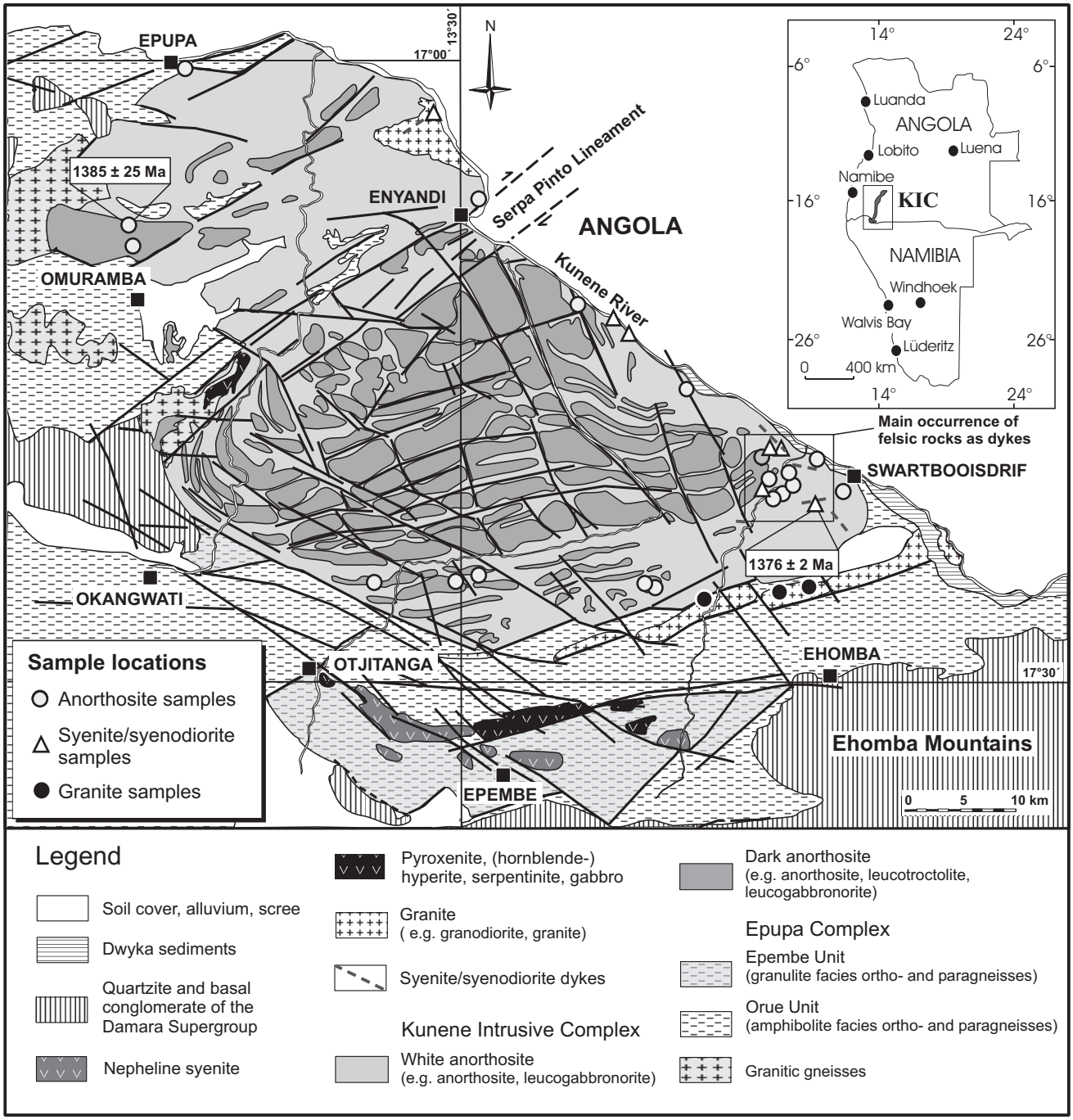
EPUPA
17°00´
13°30´
N
1385 ± 25 Ma
ENYANDI
Serpa Pinto Lineament
ANGOLA
Kunene River
OMURAMBA
14°
24°
6°
Luanda
ANGOLA
Lobito
Luena
Namibe
16°
KIC
NAMIBIA
Windhoek
Walvis Bay
26°
Lüderitz
0 400 km
Main occurrence of felsic rocks as dykes
SWARTBOOISDRIF
1376 ± 2 Ma
OKANGWATI
OTJITANGA
EHOMBA
17°30´
Ehomba Mountains
EPEMBE
0 5 10 km
Sample locations
Anorthosite samples
Syenite/syenodiorite samples
Granite samples
Legend
Soil cover, alluvium, scree
Dwyka sediments
Quartzite and basal conglomerate of the Damara Supergroup
Nepheline syenite
Pyroxenite, (hornblende-) hyperite, serpentinite, gabbro
Granite (e.g. granodiorite, granite)
Syenite/syenodiorite dykes
Kunene Intrusive Complex
White anorthosite (e.g. anorthosite, leucogabbronorite)
Dark anorthosite (e.g. anorthosite, leucotroctolite, leucogabbronorite)
Epupa Complex
Epembe Unit (granulite facies ortho- and paragneisses)
Orue Unit (amphibolite facies ortho- and paragneisses)
Granitic gneisses

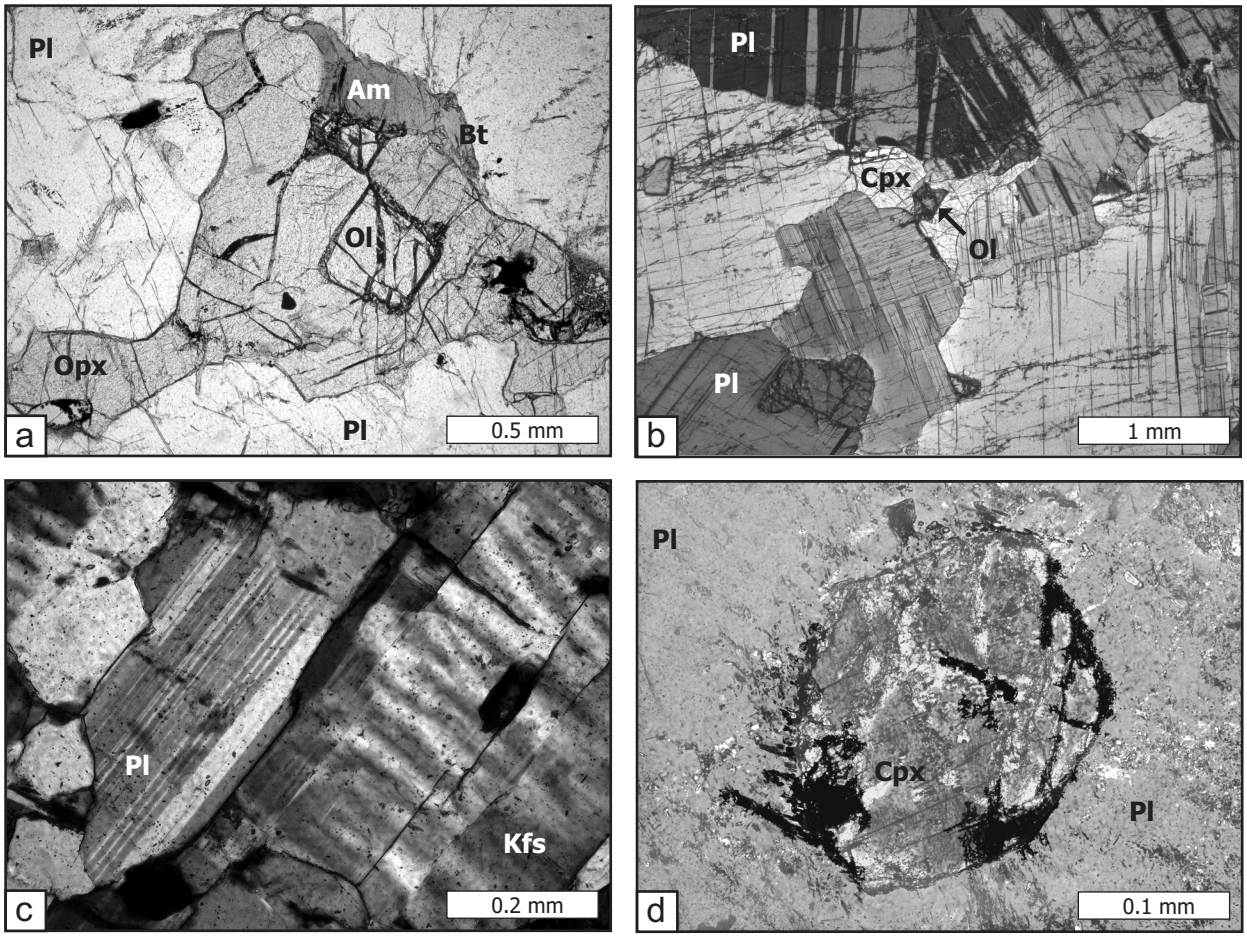
Pl
Am
Bt
Ol
Opx
Pl
0.5 mm
a
Pl
Cpx
Ol
Pl
1 mm
b
Pl
Kfs
0.2 mm
c
Pl
Cpx
Pl
0.1 mm
d

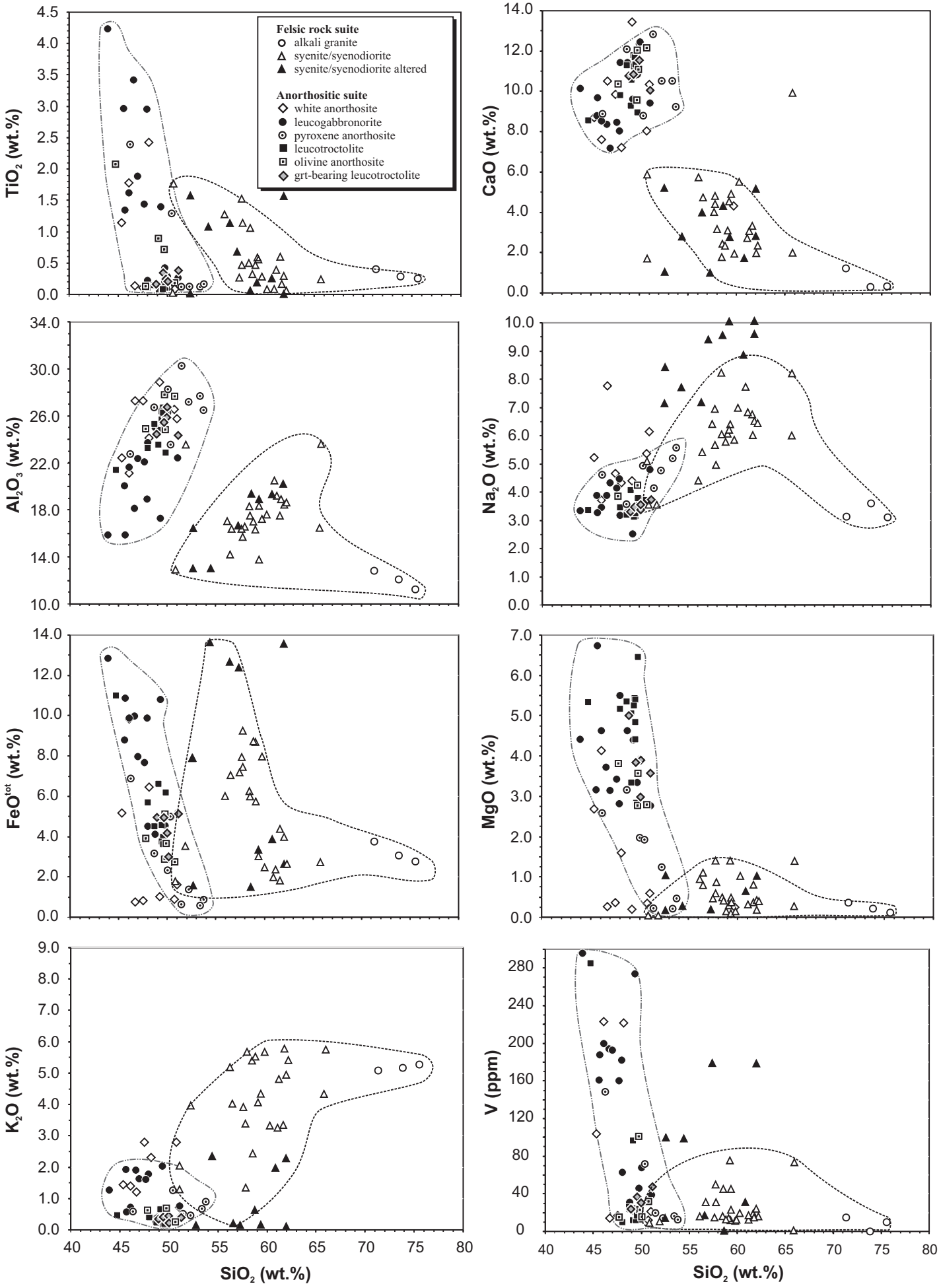
Felsic rock suite
alkali granite
syenite/syenodiorite
syenite/syenodiorite altered
Anorthositic suite
white anorthosite
leucogabbronorite
pyroxene anorthosite
leucotroctolite
olivine anorthosite
grt-bearing leucotroctolite
TiO2 (wt.%)
CaO (wt.%)
Al2O3 (wt.%)
Na2O (wt.%)
FeOtot (wt.%)
MgO (wt.%)
K2O (wt.%)
V (ppm)
SiO2 (wt.%)
SiO2 (wt.%)

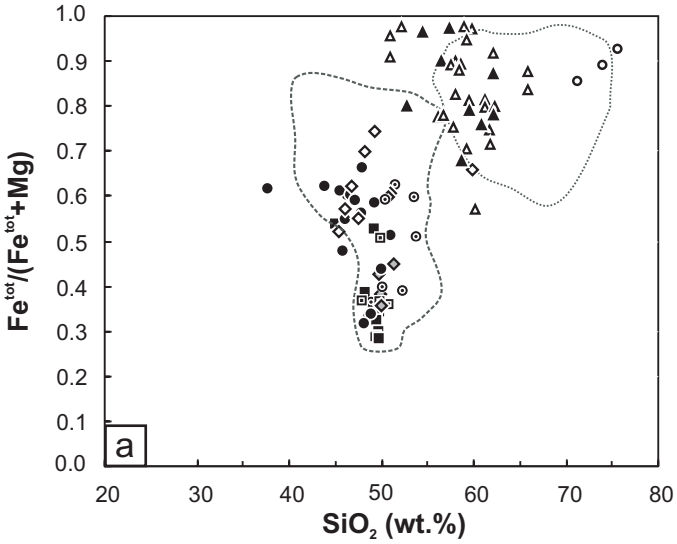
1.0
0.9
0.8
0.7
0.6
0.5
0.4
0.3
0.2
0.1
0.0
Fe^tot/(Fe^tot+Mg)
a
20
30
40
50
60
70
80
SiO2 (wt.%)

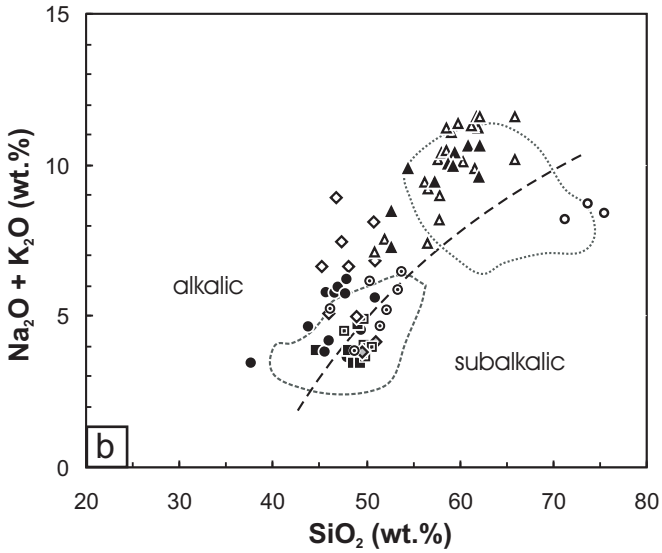
15
10
5
0
Na2O + K2O (wt.%)
alkalic
subalkalic
b
20
30
40
50
60
70
80
SiO2 (wt.%)

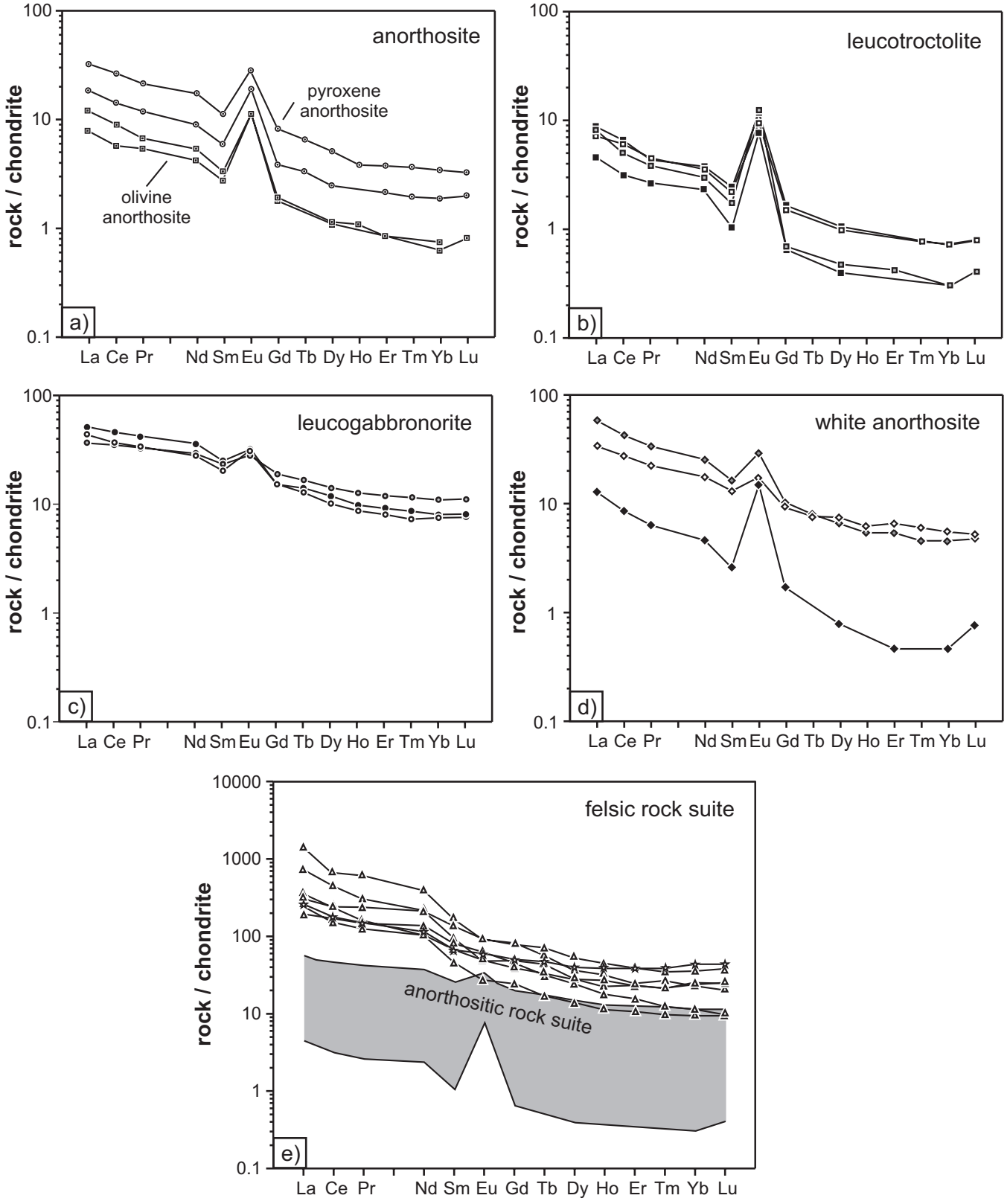
anorthosite
pyroxene anorthosite
olivine anorthosite
a)
leucotroctolite
b)
leucogabbronorite
c)
white anorthosite
d)
felsic rock suite
anorthositic rock suite
e)
rock / chondrite
100
10
1
0.1
10000
1000
La Ce Pr Nd Sm Eu Gd Tb Dy Ho Er Tm Yb Lu

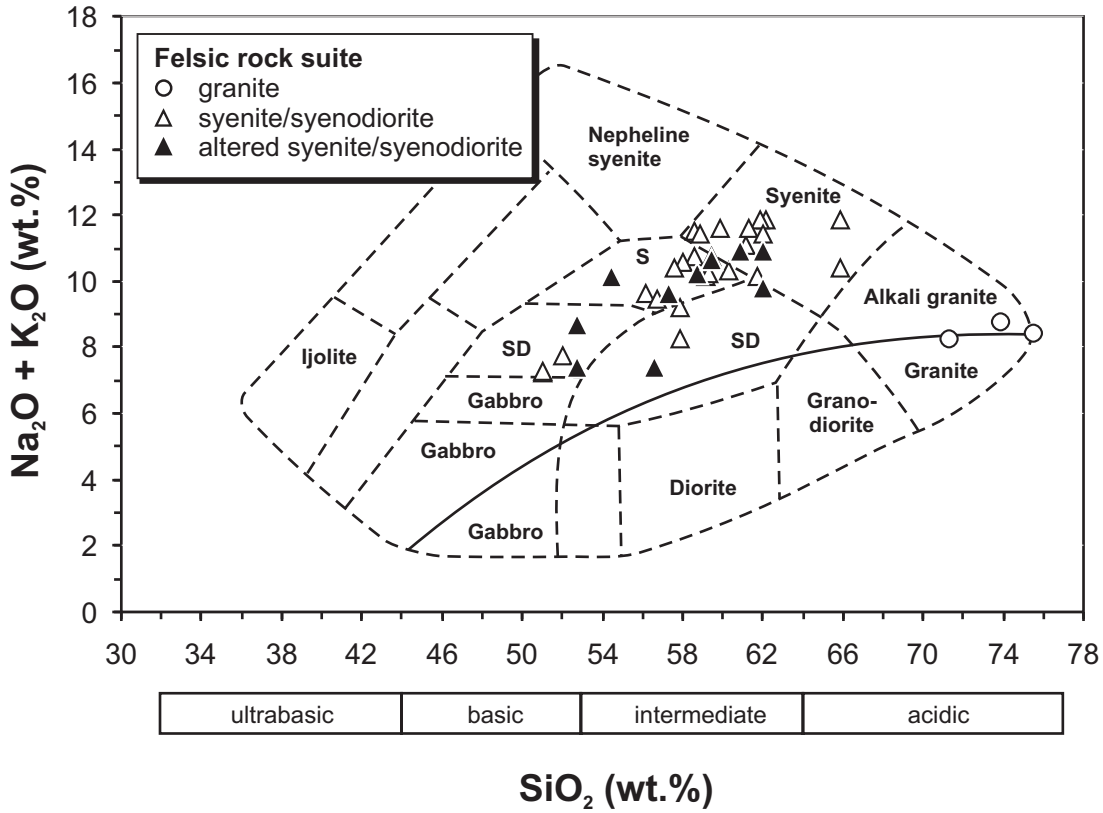
Felsic rock suite
granite
syenite/syenodiorite
altered syenite/syenodiorite
Nepheline syenite
Syenite
S
Alkali granite
SD
SD
Granite
Ijolite
Gabbro
Grano-diorite
Gabbro
Diorite
Gabbro
ultrabasic
basic
intermediate
acidic
Na2O + K2O (wt.%)
SiO2 (wt.%)

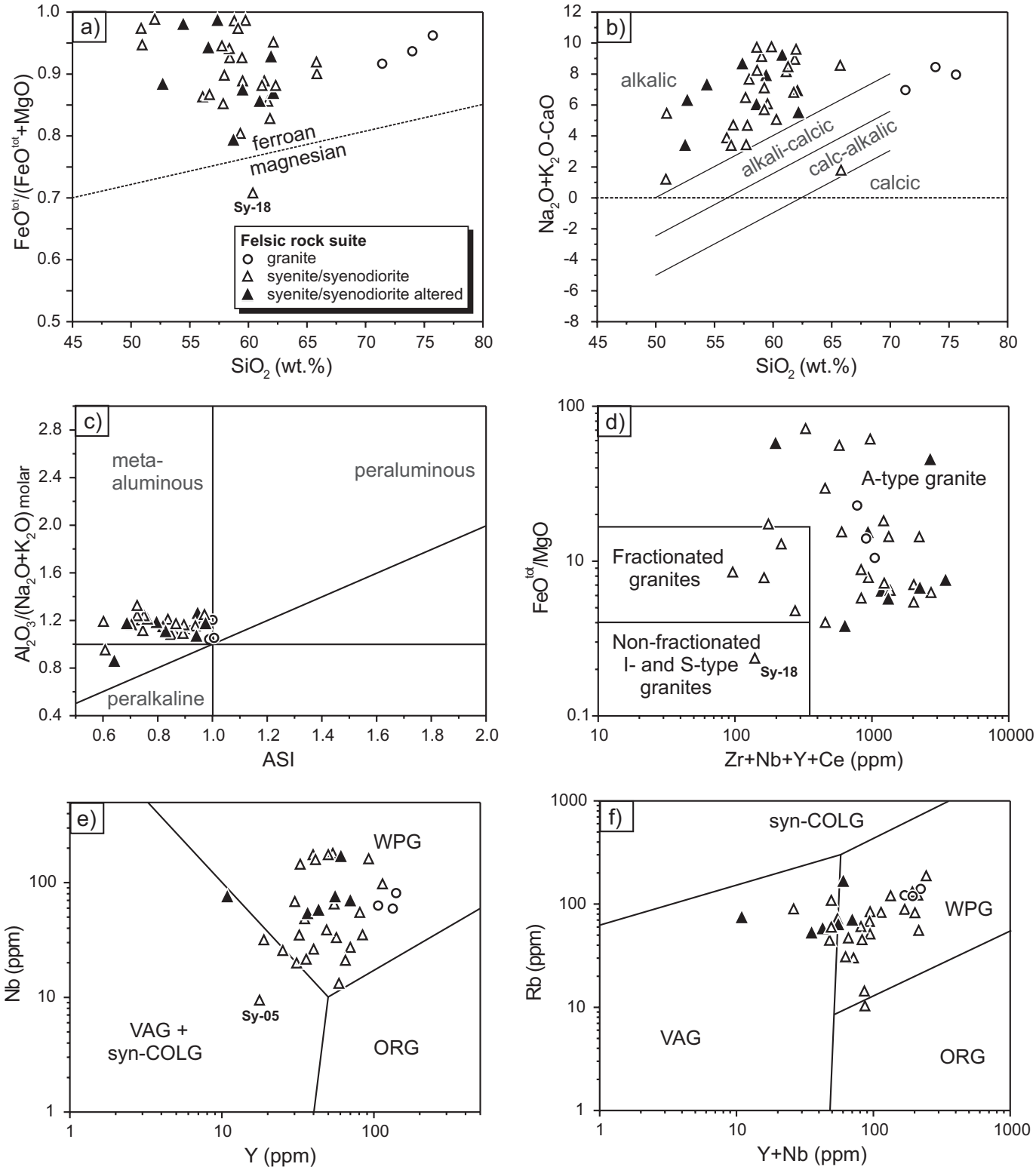
a)
FeO^tot/(FeO^tot+MgO)
SiO2 (wt.%)
ferroan
magnesian
Sy-18
Felsic rock suite
granite
syenite/syenodiorite
syenite/syenodiorite altered
b)
Na2O+K2O-CaO
SiO2 (wt.%)
alkalic
alkali-calcic
calc-alkalic
calcic
c)
Al2O3/(Na2O+K2O) molar
ASI
meta-
aluminous
peraluminous
peralkaline
d)
FeO^tot/MgO
Zr+Nb+Y+Ce (ppm)
A-type granite
Fractionated
granites
Non-fractionated
I- and S-type
granites
Sy-18
e)
Nb (ppm)
Y (ppm)
WPG
VAG +
syn-COLG
ORG
Sy-05
f)
Rb (ppm)
Y+Nb (ppm)
syn-COLG
WPG
VAG
ORG

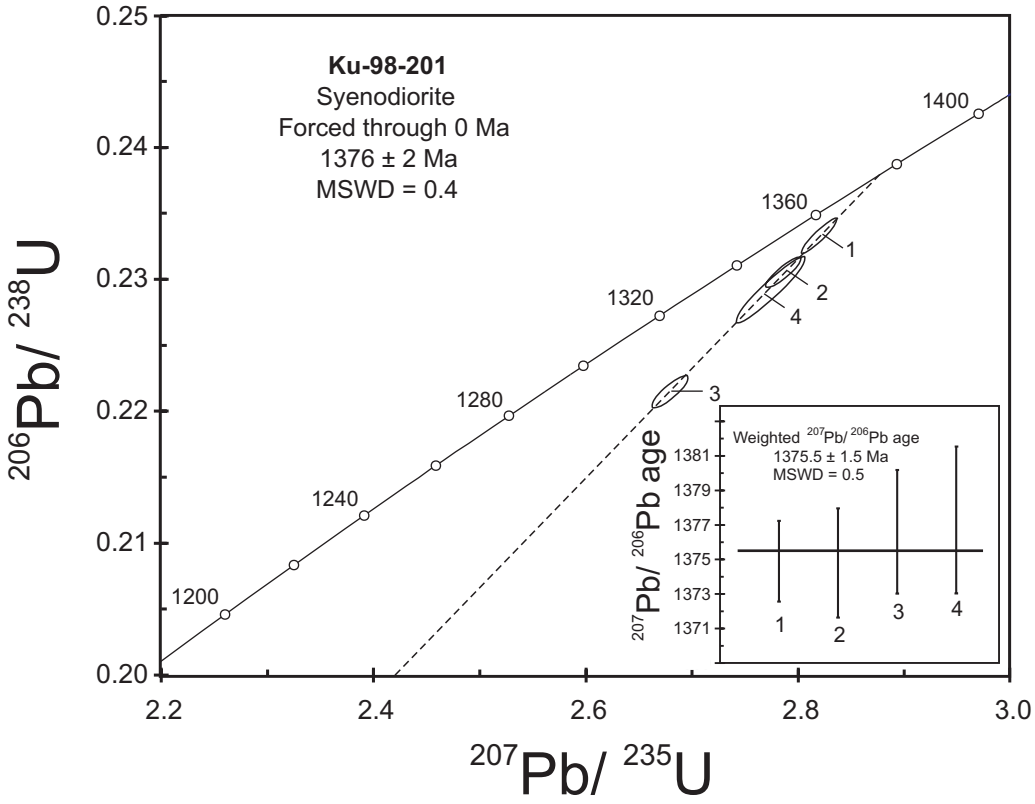
Ku-98-201
Syenodiorite
Forced through 0 Ma
1376 ± 2 Ma
MSWD = 0.4
1400
1360
1320
1280
1240
1200
1
2
3
4
Weighted 207Pb/206Pb age
1375.5 ± 1.5 Ma
MSWD = 0.5
207Pb/206Pb age
1381
1379
1377
1375
1373
1371
1
2
3
4
0.25
0.24
0.23
0.22
0.21
0.20
206Pb/238U
2.2
2.4
2.6
2.8
3.0
207Pb/235U

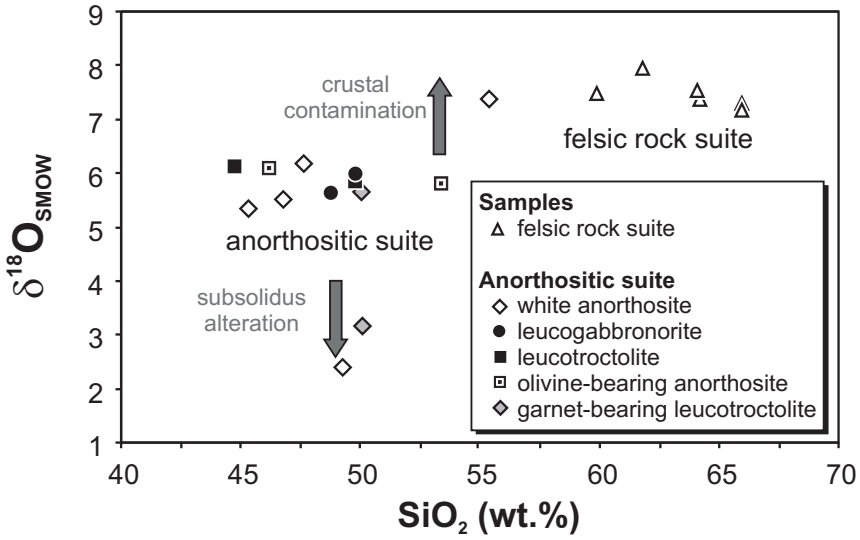
9
8
7
6
5
4
3
2
1
40
45
50
55
60
65
70
$\delta^{18}O_{SMOW}$
SiO_2 (wt.%)
crustal contamination
subsolidus alteration
anorthositic suite
felsic rock suite
Samples
felsic rock suite
Anorthositic suite
white anorthosite
leucogabbronorite
leucotroctolite
olivine-bearing anorthosite
garnet-bearing leucotroctolite

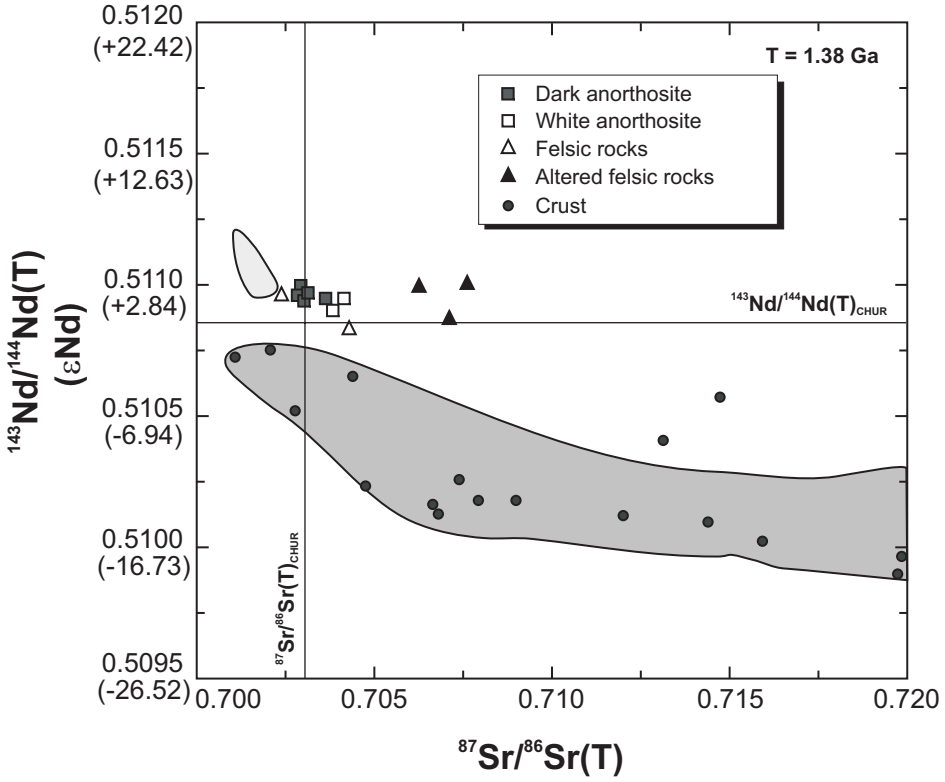
T = 1.38 Ga
Dark anorthosite
White anorthosite
Felsic rocks
Altered felsic rocks
Crust
$^{143}Nd/^{144}Nd(T)_{CHUR}$
$^{87}Sr/^{86}Sr(T)_{CHUR}$
0.5120
(+22.42)
0.5115
(+12.63)
0.5110
(+2.84)
0.5105
(-6.94)
0.5100
(-16.73)
0.5095
(-26.52)
0.700
0.705
0.710
0.715
0.720
$^{143}Nd/^{144}Nd(T)$
(εNd)
$^{87}Sr/^{86}Sr(T)$

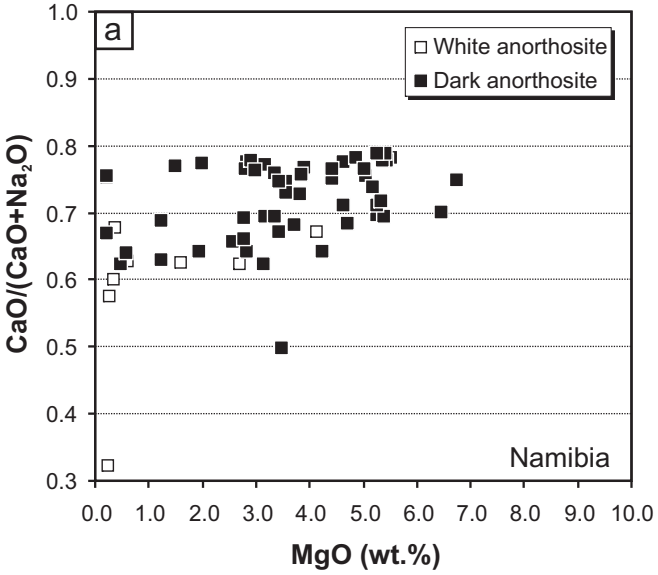
a
White anorthosite
Dark anorthosite
Namibia
CaO/(CaO+Na2O)
MgO (wt.%)
1.0
0.9
0.8
0.7
0.6
0.5
0.4
0.3
0.0 1.0 2.0 3.0 4.0 5.0 6.0 7.0 8.0 9.0 10.0

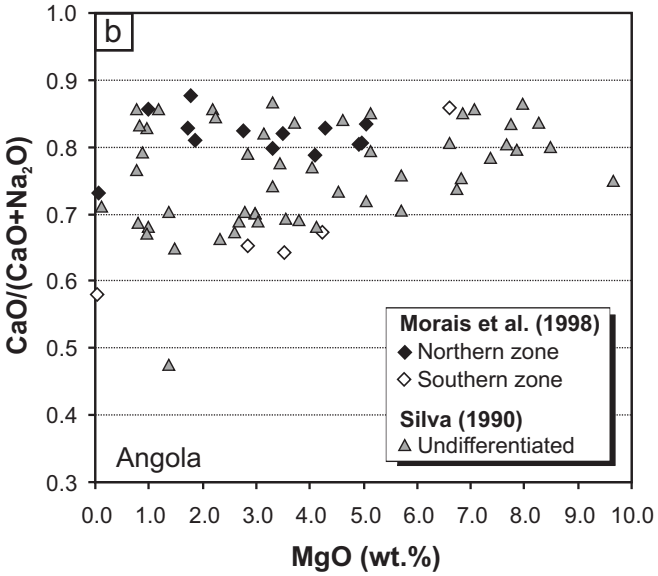
b
Morais et al. (1998)
Northern zone
Southern zone
Silva (1990)
Undifferentiated
Angola
CaO/(CaO+Na2O)
MgO (wt.%)
1.0
0.9
0.8
0.7
0.6
0.5
0.4
0.3
0.0 1.0 2.0 3.0 4.0 5.0 6.0 7.0 8.0 9.0 10.0

Table 1a. Representative electron microprobe analyses of plagioclase of the anorthosite suite.

Rock type	A,w	A,w	A,w	GN	GN	GN	GN	A,px	A,px	A,px	A,px	A,px	T	T	T	T	T	T	T	A,ol	A,ol
Sample	97-08b	97-33	97-44	97-03	98-68	98-71	98-84	97-13	97-93	97-93	98-78	98-78	97-92	97-105	98-52	98-52	98-221a	98-221b	98-221b	97-95	97-95
	fs1	fs1	fs3	fs1	fs1	fs1	fs2	fs1	fs1	fs1	fs1	fs2	fs1	fs1	fs1	fs2	fs2	fs1	fs3	fs1	fs2
Mineral	Pl	Pl	Pl	Pl	Pl	Pl	Pl	Pl	Pl	Pl	Pl	Pl	Pl	Pl	Pl	Pl	Pl	Pl	Pl	Pl	Pl
	rim	core	rim	core	rim	core	rim	rim	core	rim	core	core	rim	rim	rim	core	core	core	core	core	rim
SiO_2	54.52	67.23	57.11	55.88	54.90	54.42	50.55	55.46	53.62	54.87	54.61	53.91	54.05	52.28	55.09	55.53	52.42	57.55	53.19	53.65	54.51
Al_2O_3	28.39	20.17	26.92	27.53	28.25	29.00	31.48	27.93	29.29	28.08	28.45	29.34	29.42	30.08	27.89	27.92	29.98	27.05	29.56	28.83	29.00
MgO	0.00	0.00	0.00	0.00	0.00	0.00	0.00	0.00	0.00	0.00	0.00	0.00	0.00	0.00	0.00	0.00	0.00	0.00	0.00	0.00	0.00
CaO	10.59	0.95	8.75	9.86	10.47	10.87	14.05	10.20	11.51	10.48	10.94	11.35	11.78	12.53	10.14	9.94	12.46	9.15	12.07	11.43	11.20
MnO	0.00	0.00	0.00	0.00	0.00	0.00	0.00	0.00	0.00	0.00	0.00	0.00	0.00	0.00	0.00	0.00	0.00	0.00	0.00	0.00	0.00
FeO	0.33	0.30	0.03	0.03	0.14	0.48	0.06	0.06	0.04	0.04	0.05	0.06	0.13	0.13	0.09	0.06	0.04	0.18	0.13	0.13	0.01
BaO	0.04	0.00	0.05	0.09	0.01	0.10	0.00	0.04	0.03	0.02	0.00	0.00	0.00	0.02	0.06	0.04	0.07	0.00	0.02	0.00	0.04
Na_2O	5.39	11.13	6.43	5.91	5.52	5.27	3.49	5.80	4.88	5.50	5.35	5.04	4.81	4.25	5.72	5.82	4.32	6.30	4.67	4.99	5.24
K_2O	0.05	0.03	0.07	0.08	0.11	0.17	0.00	0.04	0.07	0.06	0.11	0.12	0.27	0.21	0.08	0.14	0.14	0.21	0.04	0.03	0.07
Sum	99.32	99.81	99.36	99.38	99.41	100.31	99.62	99.53	99.43	99.05	99.51	99.82	100.45	99.48	99.07	99.45	99.43	100.45	99.69	99.05	100.06
Formula (O=8)																					
Si	2.48	2.95	2.57	2.53	2.49	2.45	2.31	2.51	2.44	2.49	2.47	2.44	2.43	2.38	2.50	2.51	2.39	2.57	2.41	2.45	2.46
Al	1.52	1.04	1.43	1.47	1.51	1.54	1.69	1.49	1.57	1.50	1.52	1.56	1.56	1.62	1.49	1.49	1.61	1.42	1.58	1.55	1.54
Mg	0.00	0.00	0.00	0.00	0.00	0.00	0.00	0.00	0.00	0.00	0.00	0.00	0.00	0.00	0.00	0.00	0.00	0.00	0.00	0.00	0.00
Ca	0.52	0.04	0.42	0.48	0.51	0.53	0.69	0.49	0.56	0.51	0.53	0.55	0.57	0.61	0.49	0.48	0.61	0.44	0.59	0.56	0.54
Mn	0.00	0.00	0.00	0.00	0.00	0.00	0.00	0.00	0.00	0.00	0.00	0.00	0.00	0.00	0.00	0.00	0.00	0.00	0.00	0.00	0.00
Fe	0.01	0.01	0.00	0.00	0.01	0.02	0.00	0.00	0.00	0.00	0.00	0.00	0.00	0.00	0.00	0.00	0.00	0.01	0.00	0.00	0.00
Ba	0.00	0.00	0.00	0.00	0.00	0.00	0.00	0.00	0.00	0.00	0.00	0.00	0.00	0.00	0.00	0.00	0.00	0.00	0.00	0.00	0.00
Na	0.47	0.95	0.56	0.52	0.49	0.46	0.31	0.51	0.43	0.48	0.47	0.44	0.42	0.38	0.50	0.51	0.38	0.55	0.41	0.44	0.46
K	0.00	0.00	0.00	0.00	0.01	0.01	0.00	0.00	0.00	0.00	0.01	0.01	0.02	0.01	0.00	0.01	0.01	0.01	0.00	0.00	0.00
Sum	5.00	5.00	4.99	5.00	5.00	5.01	5.00	5.00	5.00	5.00	5.00	5.00	5.00	5.00	5.00	5.00	5.00	5.00	5.00	5.00	5.00
Si+Al	4.00	4.00	4.00	4.00	4.00	4.00	4.00	4.00	4.00	4.00	3.99	4.00	4.00	4.00	4.00	4.00	4.00	3.99	4.00	4.00	4.00
Na+Ca+K	0.99	0.99	0.99	1.00	1.00	1.00	1.00	1.01	0.99	1.00	1.01	1.00	1.00	1.00	1.00	1.00	1.00	1.00	1.00	1.00	1.00
AN(Na/Ca)	51.84	4.49	42.69	47.66	50.82	52.62	68.95	49.11	56.33	51.08	52.76	55.09	56.62	61.21	49.20	48.14	60.87	43.97	58.65	55.79	53.91
AB(Na/Ca)	47.78	95.35	56.79	51.74	48.51	46.21	31.04	50.58	43.23	48.54	46.63	44.23	41.83	37.56	50.24	50.99	38.21	54.81	41.06	44.05	45.62
OR	0.31	0.16	0.42	0.44	0.65	0.99	0.01	0.24	0.40	0.34	0.60	0.69	1.56	1.19	0.45	0.80	0.80	1.22	0.25	0.16	0.40
CE	0.07	0.00	0.09	0.16	0.02	0.18	0.00	0.07	0.05	0.04	0.00	0.00	0.00	0.04	0.11	0.07	0.13	0.00	0.04	0.00	0.07

Abbrevations: *A,w* white anorthosite; *A,ol* olivine anorthosite; *A,px* pyroxene anorthosite; *GN* leucogabbronorite; *T* leucotroctolite.

Table 1b. Representative electron microprobe analyses of plagioclase of the felsic rock suite.

Sample	98-07	98-40	98-40	99-11	99-11	99-11	99-11	99-12	99-13	99-13	99-13	99-14
	3-fs4	2-fs1	2-fs1	a-fs1	a-fs1	a-fs2	a-fs2	b-fs4	1-fs2	3-fs3	3-fs3	a-fs2
Mineral	Pl	Pl	Pl	Pl	Pl	Pl	Pl	Pl	Pl	Pl	Pl	Pl
	rim	rim	core	core	core	core	core	rim	rim	rim	->	core
SiO_2	67.32	69.02	64.11	65.27	66.07	64.88	65.58	66.99	66.55	67.97	66.92	67.12
Al_2O_3	19.85	19.71	22.87	21.12	21.18	21.32	21.15	20.24	19.80	19.95	20.02	20.57
MgO	0.00	0.01	0.00	0.00	0.02	0.00	0.00	0.02	0.03	0.00	0.00	0.00
CaO	0.27	0.17	3.73	1.96	1.86	2.36	2.11	0.85	0.58	0.59	0.88	0.94
MnO	0.00	0.00	0.00	0.00	0.00	0.00	0.00	0.00	0.00	0.00	0.00	0.00
FeO	0.05	0.07	0.10	0.20	0.24	0.17	0.12	0.05	0.33	0.16	0.06	0.04
BaO	0.00	0.04	0.00	0.07	0.00	0.05	0.00	0.00	0.00	0.00	0.04	0.08
Na_2O	11.62	11.78	9.57	10.46	10.66	10.18	10.32	11.25	11.20	11.36	11.12	10.96
K_2O	0.03	0.15	0.32	0.14	0.12	0.20	0.13	0.08	0.06	0.10	0.11	0.17
Sum	99.14	100.95	100.69	99.22	100.16	99.15	99.40	99.48	98.55	100.12	99.16	99.88
Formula (O=8)												
Si	2.97	2.99	2.81	2.89	2.90	2.88	2.90	2.95	2.96	2.97	2.96	2.94
Al	1.03	1.01	1.18	1.10	1.10	1.12	1.10	1.05	1.04	1.03	1.04	1.06
Mg	0.00	0.00	0.00	0.00	0.00	0.00	0.00	0.00	0.00	0.00	0.00	0.00
Ca	0.01	0.01	0.18	0.09	0.09	0.11	0.10	0.04	0.03	0.03	0.04	0.04
Mn	0.00	0.00	0.00	0.00	0.00	0.00	0.00	0.00	0.00	0.00	0.00	0.00
Fe	0.00	0.00	0.00	0.01	0.01	0.01	0.00	0.00	0.01	0.01	0.00	0.00
Ba	0.00	0.00	0.00	0.00	0.00	0.00	0.00	0.00	0.00	0.00	0.00	0.00
Na	0.99	0.99	0.81	0.90	0.91	0.88	0.88	0.96	0.97	0.96	0.95	0.93
K	0.00	0.01	0.02	0.01	0.01	0.01	0.01	0.00	0.00	0.01	0.01	0.01
Sum	5.01	5.01	5.01	5.01	5.01	5.00	5.00	5.01	5.01	5.00	5.00	5.00
Si+Al	4.00	4.00	4.00	4.00	4.00	4.00	4.00	4.00	4.00	4.00	4.00	4.01
Na+Ca+K	1.01	1.01	1.01	1.00	1.00	1.00	0.99	1.00	1.00	1.00	1.00	0.99
AN(Na/Ca)	1.26	0.76	17.43	9.29	8.74	11.23	10.07	3.99	2.79	2.78	4.16	4.48
AB(Na/Ca)	98.55	98.36	80.81	89.81	90.57	87.57	89.18	95.57	96.89	96.64	95.14	94.42
OR	0.18	0.82	1.76	0.79	0.69	1.11	0.76	0.44	0.32	0.58	0.64	0.96
CE	0.00	0.06	0.00	0.12	0.00	0.09	0.00	0.00	0.00	0.00	0.07	0.13

Table 2. Representative electron microprobe analyses of pyroxene of the anorthosite and the felsic rock suites.

Rock type	Leucogabbronorite		Leucotroctolite				Felsic rocks		White anorthosite	Leucotroctolite					
Sample	Ku-97-03 cpx1 core	Ku-97-04 cpx1 rim	Ku-97-92 cpx1 rim	Ku-97-105 cpx1 core	Ku-98-52 cpx2 rim	Ku-98-221a cpx1 core	Ku-98-40 7-cpx1 rim	Ku-98-40 7-cpx2 ->	Ku-97-33 opx1 core	Ku-97-92 opx1 core	Ku-97-104 opx1 core	Ku-97-105 opx1 core	Ku-97-52 opx1 rim	Ku-98-221a opx1 ->	Ku-98-221b opx1 olivine
SiO_2	51.04	51.37	48.95	50.30	51.11	51.29	50.22	51.08	53.70	52.19	54.52	53.13	52.02	52.74	53.36
TiO_2	0.42	0.23	0.99	0.81	0.36	0.43	0.08	0.05	0.06	0.12	0.00	0.24	0.20	0.21	0.00
Al_2O_3	1.71	1.55	5.45	3.16	1.67	2.27	0.62	0.41	0.22	3.24	0.68	1.58	1.55	1.59	0.48
Cr_2O_3	0.01	0.00	0.09	0.14	0.03	0.00	0.02	0.01	0.03	0.01	0.01	0.02	0.01	0.00	0.01
MgO	11.54	9.84	13.03	13.35	12.38	14.21	7.96	8.69	25.84	24.73	26.13	24.75	20.98	22.91	24.99
CaO	21.96	22.53	21.99	21.97	21.78	23.11	20.99	21.50	0.09	0.59	0.12	0.76	0.86	0.96	0.14
MnO	0.29	0.47	0.21	0.22	0.53	0.22	1.49	1.49	0.37	0.31	0.29	0.40	0.68	0.39	0.44
FeO	11.56	13.11	8.06	9.00	11.22	7.99	17.23	15.62	18.34	18.58	18.59	18.29	23.45	21.58	19.62
Na_2O	0.51	0.80	0.68	0.37	0.33	0.26	0.56	0.66	0.00	0.00	0.00	0.02	0.08	0.00	0.00
K_2O	0.02	0.00	0.00	0.00	0.02	0.00	0.02	0.00	0.01	0.01	0.01	0.01	0.00	0.00	0.02
Total	99.07	99.89	99.44	99.33	99.43	99.78	99.18	99.50	98.66	99.78	100.35	99.19	99.82	100.37	99.05
Formula (O=6)															
Si	1.95	1.97	1.84	1.90	1.94	1.92	1.98	1.99	1.99	1.91	1.98	1.96	1.96	1.95	1.98
Al	0.05	0.03	0.16	0.10	0.06	0.08	0.02	0.01	0.01	0.09	0.02	0.04	0.04	0.05	0.02
Sum Z	2.00	2.00	2.00	2.00	2.00	2.00	2.00	2.00	2.00	2.00	2.00	2.00	2.00	2.00	2.00
Al	0.03	0.04	0.08	0.04	0.02	0.02	0.01	0.01	0.00	0.05	0.01	0.03	0.02	0.02	0.00
Cr	0.00	0.00	0.00	0.00	0.00	0.00	0.00	0.00	0.00	0.00	0.00	0.00	0.00	0.00	0.00
Ti	0.01	0.01	0.03	0.02	0.01	0.01	0.00	0.00	0.00	0.00	0.00	0.01	0.01	0.01	0.00
Mg	0.66	0.56	0.73	0.75	0.70	0.79	0.47	0.50	1.00	0.94	0.99	0.97	0.97	0.97	1.00
Fe^{2+}	0.30	0.40	0.16	0.18	0.27	0.17	0.52	0.48	0.00	0.00	0.00	0.00	0.00	0.00	0.00
Mn	0.00	0.00	0.00	0.00	0.00	0.00	0.00	0.00	0.00	0.00	0.00	0.00	0.00	0.00	0.00
Sum Y	1.00	1.00	1.00	1.00	1.00	1.00	1.00	1.00	1.00	1.00	1.00	1.00	1.00	1.00	1.00
Mg	0.00	0.00	0.00	0.00	0.00	0.00	0.00	0.00	0.43	0.41	0.43	0.39	0.21	0.29	0.38
Fe^{2+}	0.07	0.02	0.09	0.10	0.09	0.08	0.05	0.03	0.57	0.57	0.56	0.56	0.74	0.67	0.61
Mn	0.01	0.02	0.01	0.01	0.02	0.01	0.05	0.05	0.01	0.01	0.01	0.01	0.02	0.01	0.01
Ca	0.90	0.92	0.89	0.89	0.89	0.93	0.89	0.90	0.00	0.02	0.00	0.03	0.03	0.04	0.01
Na	0.04	0.06	0.05	0.03	0.02	0.02	0.04	0.05	0.00	0.00	0.00	0.00	0.01	0.00	0.00
K	0.00	0.00	0.00	0.00	0.00	0.00	0.00	0.00	0.00	0.00	0.00	0.00	0.00	0.00	0.00
Sum X	1.02	1.02	1.04	1.02	1.02	1.03	1.03	1.02	1.01	1.01	1.00	1.00	1.01	1.01	1.01
Total	4.02	4.02	4.04	4.02	4.02	4.03	4.03	4.02	4.01	4.01	4.00	4.00	4.01	4.01	4.01

Table 3. Representative electron microprobe analyses of amphibole of the anorthosite and the felsic rock suites.

Rock type	Leucogabbronorite				White anorthosite		Px anorthosite		Felsic rock suite					
Sample	Ku-97-03 am1	Ku-97-03 am8	Ku-97-04 am1	Ku-97-04 am4	Ku-97-08b am1	Ku-97-08b am3	Ku-97-13 am1	Ku-97-13 am2	Ku-99-11 a-am2	Ku-99-11 a-am2	Ku-99-13 3-am1	Ku-99-13 3-am1	Ku-99-14 a-am1	Ku-99-14 a-am1
SiO_2	40.73	41.41	39.07	40.63	41.69	39.82	40.65	43.24	36.79	36.72	37.51	36.67	36.89	36.89
TiO_2	3.24	2.92	3.43	2.45	0.73	1.89	0.80	0.16	1.87	1.94	0.80	0.75	0.70	0.76
Al_2O_3	11.90	11.88	12.84	11.16	14.29	14.83	12.21	10.22	10.33	10.23	9.86	10.26	10.84	10.78
Cr_2O_3	0.03	0.00	0.01	0.00	0.00	0.05	0.00	0.01	0.00	0.03	0.00	0.00	0.00	0.05
Fe_2O_3	1.19	0.84	0.23	1.01	4.07	3.43	4.55	5.54	9.27	10.53	11.52	13.70	11.79	11.92
FeO	14.52	13.58	19.17	18.43	10.12	10.53	16.17	14.34	22.68	22.24	21.80	20.85	21.51	21.63
MgO	10.28	10.81	7.10	8.26	11.88	11.50	7.83	9.65	0.42	0.48	0.40	0.23	0.37	0.31
MnO	0.19	0.15	0.26	0.31	0.19	0.21	0.20	0.26	0.83	0.88	0.95	1.05	1.08	1.05
CaO	11.03	11.26	11.16	11.22	11.21	10.90	11.53	11.62	10.46	10.63	9.72	10.27	10.49	10.40
Na_2O	2.43	2.18	2.34	2.23	2.05	2.68	1.33	1.32	1.81	1.94	2.09	2.42	2.21	2.20
K_2O	1.07	0.97	1.31	1.43	1.00	0.66	1.03	0.74	1.75	1.76	1.91	1.96	2.21	2.22
Total	96.59	95.99	96.91	97.12	97.23	96.47	96.30	97.09	96.21	97.37	96.56	98.16	98.08	98.20
Formula (O=23)														
Si	6.20	6.29	6.07	6.28	6.17	5.97	6.28	6.55	6.07	6.00	6.16	5.97	6.00	5.99
Ti	0.37	0.33	0.40	0.28	0.08	0.21	0.09	0.02	0.23	0.24	0.10	0.09	0.09	0.09
Al	2.13	2.12	2.35	2.03	2.49	2.62	2.22	1.82	2.01	1.97	1.91	1.97	2.08	2.06
Cr	0.00	0.00	0.00	0.00	0.00	0.01	0.00	0.00	0.00	0.00	0.00	0.00	0.00	0.01
Fe^{3+}	0.14	0.10	0.03	0.12	0.45	0.39	0.53	0.63	1.15	1.29	1.42	1.68	1.44	1.46
Fe^{2+}	1.85	1.72	2.49	2.38	1.25	1.32	2.09	1.82	3.13	3.04	3.00	2.84	2.92	2.94
Mg	2.33	2.45	1.64	1.90	2.62	2.57	1.80	2.18	0.10	0.12	0.10	0.06	0.09	0.08
Mn	0.02	0.02	0.03	0.04	0.02	0.03	0.03	0.03	0.12	0.12	0.13	0.14	0.15	0.14
Ca	1.80	1.83	1.86	1.86	1.78	1.75	1.91	1.89	1.85	1.86	1.71	1.79	1.83	1.81
Na	0.72	0.64	0.70	0.67	0.59	0.78	0.40	0.39	0.58	0.61	0.66	0.76	0.70	0.69
K	0.21	0.19	0.26	0.28	0.19	0.13	0.20	0.14	0.37	0.37	0.40	0.41	0.46	0.46
Total	15.76	15.69	15.83	15.84	15.66	15.76	15.55	15.47	15.60	15.62	15.60	15.70	15.74	15.73
X_{Mg}	0.56	0.59	0.40	0.44	0.68	0.66	0.46	0.55	0.03	0.04	0.03	0.02	0.03	0.02

Table 4. Selected major and trace element data of the anorthosite and the felsic rock suites.

Rock type	A,w	A,w	A,w	A,px	A,px	A,ol	A,ol	GN	GN	GN	GN	T	T	T	T,grt	G	S	S	S	SD,a	SD,a	SD,a
Sample	97-33b	97-44	98-45	97-13	97-31	97-28	98-23	97-04	97-05	97-31b	98-68	97-92	98-41	98-230	97-104	98-180a	98-40	99-20	Sy-25	98-201	98-200	98-204
wt.%																						
SiO_2	47.51	51.03	49.22	50.41	46.23	49.87	49.77	43.91	47.95	37.67	51.09	49.82	49.47	49.41	48.93	75.56	65.80	61.64	59.29	56.51	62.00	51.97
TiO_2	0.11	0.38	0.13	1.29	2.39	0.12	0.19	4.24	2.95	7.25	0.27	0.11	0.13	0.08	0.15	0.25	0.25	0.61	0.61	1.16	0.05	0.04
Al_2O_3	27.27	25.78	28.85	23.53	22.79	26.27	27.77	15.85	18.91	17.26	22.41	22.89	25.70	26.38	24.52	11.27	16.44	17.52	13.80	14.18	20.11	23.43
Fe_2O_3	0.77	1.53	0.85	1.62	2.25	1.20	0.90	4.00	2.60	3.92	1.35	1.54	0.86	0.93	1.31	1.53	1.87	2.08	6.38	14.16	2.95	4.02
FeO	0.11	0.22	0.25	3.50	4.87	2.59	2.05	9.24	7.54	11.38	3.95	4.81	3.80	2.91	3.71	1.38	1.02	2.52	n.a.	n.a.	n.a.	n.a.
MnO	0.03	0.04	0.03	0.08	0.08	0.05	0.04	0.25	0.25	0.18	0.05	0.07	0.07	0.05	0.07	0.05	0.05	0.09	0.15	0.22	0.04	0.14
MgO	0.37	0.59	0.20	1.92	2.57	3.56	2.81	4.42	2.82	5.25	2.77	6.46	5.43	5.25	5.00	0.12	0.30	0.80	1.41	0.82	0.41	0.05
CaO	9.84	10.35	13.43	8.81	8.86	11.08	12.03	10.14	8.04	7.52	9.42	8.96	11.22	11.78	10.76	0.33	2.00	3.32	4.50	4.03	2.83	9.99
Na_2O	4.65	6.13	4.40	4.91	4.62	3.73	3.45	3.35	4.47	3.05	4.80	3.80	3.19	3.14	3.28	3.11	6.07	6.76	6.15	7.20	9.68	3.62
K_2O	2.80	0.71	0.52	1.25	0.60	0.27	0.23	1.27	1.78	0.44	0.77	0.51	0.27	0.17	0.36	5.28	4.33	3.34	4.03	0.19	0.07	4.06
P_2O_5	0.01	0.11	0.01	0.20	0.06	0.01	0.03	0.16	0.12	0.03	0.45	0.02	0.01	0.01	0.01	0.12	0.05	0.19	0.18	0.27	0.14	0.03
S	b.d.l.	b.d.l.	0.02	0.04	0.08	b.d.l.	0.02	0.16	0.06	0.19	0.02	b.d.l.	0.02	0.02	b.d.l.	b.d.l.	b.d.l.	b.d.l.	<0.02	0.03	<0.02	<0.02
GV	5.83	3.09	2.30	1.45	3.61	0.85	1.26	1.61	1.68	4.73	2.15	0.42	0.27	0.31	1.21	0.37	0.95	0.62	3.17	0.40	0.79	1.66
CO_2	n.a.	n.a.	n.a.	n.a.	n.a.	n.a.	n.a.	n.a.	n.a.	n.a.	n.a.	n.a.	n.a.	n.a.	n.a.	n.a.	0.65	0.42	n.a.	n.a.	n.a.	n.a.
H_2O	n.a.	n.a.	n.a.	n.a.	n.a.	n.a.	n.a.	n.a.	n.a.	n.a.	n.a.	n.a.	n.a.	n.a.	n.a.	n.a.	0.30	0.20	n.a.	n.a.	n.a.	n.a.
Total	99.31	99.97	100.22	99.01	99.01	99.60	100.54	98.60	99.17	98.88	99.50	99.42	100.44	100.44	99.32	99.37	99.12	99.49	99.67	99.17	99.07	99.01
ppm																						
Sc	b.d.l.	b.d.l.	b.d.l.	b.d.l.	b.d.l.	b.d.l.	b.d.l.	b.d.l.	b.d.l.	b.d.l.	15	b.d.l.	b.d.l.	b.d.l.	b.d.l.	b.d.l.	b.d.l.	17	13	22	2.4	0.92
V	17	21	22	72	148	16	23	296	182	317	39	13	25	12	25	10	b.d.l.	19	76	17	24	13
Cr	b.d.l.	13	b.d.l.	11	46	12	15	36	25	70	12	24	24	27	46	b.d.l.	b.d.l.	b.d.l.	20	<10	<10	<10
Co	21	53	54	56	56	56	45	62	47	96	46	104	58	45	64	71	138	43	<10	12	<10	<10
Ni	b.d.l.	26	b.d.l.	23	70	94	75	36	34	159	36	187	157	185	119	b.d.l.	b.d.l.	6	<5	<5	<5	<5
Zn	45	16	b.d.l.	59	92	33	18	118	83	138	44	52	33	22	39	99	62	54	82	532	32	37
Ga	b.d.l.	b.d.l.	19	b.d.l.	b.d.l.	b.d.l.	29	b.d.l.	b.d.l.	b.d.l.	17	b.d.l.	25	26	b.d.l.	34	31	42	9	26	31	43
Rb	69	9	b.d.l.	21	9	5	b.d.l.	28	33	10	12	5	b.d.l.	b.d.l.	6	121	116	82	88	7	<5	109
Sr	805	805	627	685	642	475	566	447	510	423	979	535	520	543	470	26	201	266	674	199	1309	4514
Y	13	11	b.d.l.	10	8	8	b.d.l.	19	16	8	13	8	b.d.l.	b.d.l.	8	107	79	84	33	72	62	19
Zr	28	59	b.d.l.	63	48	19	b.d.l.	104	99	107	39	18	b.d.l.	b.d.l.	19	617	694	1854	284	791	977	284
Nb	10	7	b.d.l.	5	5	5	b.d.l.	15	17	13	b.d.l.	5	b.d.l.	b.d.l.	5	63	55	34	138	68	163	32
Mo	b.d.l.	b.d.l.	b.d.l.	b.d.l.	b.d.l.	b.d.l.	b.d.l.	b.d.l.	b.d.l.	b.d.l.	b.d.l.	b.d.l.	b.d.l.	b.d.l.	b.d.l.	239	b.d.l.	b.d.l.	7	13	b.d.l.	b.d.l.
Ba	1510	555	236	706	409	121	134	567	662	355	773	245	124	99	164	b.d.l.	1448	900	543	792	194	1013
Pb	b.d.l.	b.d.l.	b.d.l.	b.d.l.	b.d.l.	b.d.l.	b.d.l.	b.d.l.	b.d.l.	b.d.l.	8	b.d.l.	b.d.l.	b.d.l.	b.d.l.	25	29	25	28	14	21	59
Th	b.d.l.	b.d.l.	b.d.l.	b.d.l.	b.d.l.	b.d.l.	b.d.l.	b.d.l.	b.d.l.	b.d.l.	b.d.l.	b.d.l.	b.d.l.	b.d.l.	b.d.l.	b.d.l.	13	b.d.l.	b.d.l.	b.d.l.	121	19
U	b.d.l.	b.d.l.	b.d.l.	b.d.l.	b.d.l.	b.d.l.	b.d.l.	b.d.l.	b.d.l.	b.d.l.	b.d.l.	b.d.l.	b.d.l.	b.d.l.	b.d.l.	b.d.l.	b.d.l.	b.d.l.	b.d.l.	b.d.l.	16	11
Ce	b.d.l.	b.d.l.	b.d.l.	b.d.l.	b.d.l.	b.d.l.	b.d.l.	b.d.l.	b.d.l.	b.d.l.	b.d.l.	b.d.l.	b.d.l.	b.d.l.	b.d.l.	b.d.l.	150	184	b.d.l.	b.d.l.	b.d.l.	b.d.l.
Nd	b.d.l.	b.d.l.	b.d.l.	b.d.l.	b.d.l.	b.d.l.	b.d.l.	b.d.l.	b.d.l.	b.d.l.	b.d.l.	b.d.l.	b.d.l.	b.d.l.	b.d.l.	b.d.l.	70	91	b.d.l.	b.d.l.	b.d.l.	b.d.l.

Abbrevations: *A,w* white anorthosite; *A,ol* olivine anorthosite; *A,px* pyroxene anorthosite; *b.d.l.* below detection limit; *G* granite; *GN* leucogabbronorite; *n.a.* not analysed; *S* syenite; *SD* syenodiorite.

Table 5. Rare earth element data of the anorthosite and the felsic rock suites.

Rock type	A,w	A,w	A,w	A,px	A,px	A,ol	A,ol	T	T	T	T
Sample	97-33b	97-44	98-45	97-13	97-31	97-28	98-23	97-92	97-104	98-41	98-230
ppm											
Y	11.00	8.30	1.10	6.10	3.10	1.30	1.20	0.40	1.20	1.20	0.43
La	8.10	14.00	3.20	7.40	4.40	2.90	1.90	2.00	2.20	1.80	1.10
Ce	17.00	27.00	5.50	16.00	8.70	5.70	3.60	3.20	4.20	3.90	2.00
Pr	2.10	3.20	0.62	2.00	1.10	0.64	0.50	0.37	0.43	0.43	0.25
Nd	8.30	12.00	2.30	8.20	4.30	2.50	2.00	1.40	1.80	1.70	1.10
Sm	2.00	2.50	0.41	1.70	0.89	0.49	0.40	0.27	0.38	0.34	0.16
Eu	1.00	1.70	0.91	1.60	1.08	0.63	0.63	0.71	0.69	0.54	0.44
Gd	1.90	2.10	0.37	1.60	0.76	0.39	0.35	0.14	0.34	0.31	0.13
Tb	0.28	0.30	b.d.l.	0.23	0.12	b.d.l.	b.d.l.	b.d.l.	b.d.l.	b.d.l.	b.d.l.
Dy	1.90	1.70	0.21	1.30	0.63	0.28	0.27	0.12	0.27	0.25	0.10
Ho	0.36	0.31	b.d.l.	0.21	b.d.l.	0.06	b.d.l.	b.d.l.	b.d.l.	b.d.l.	b.d.l.
Er	1.10	0.89	0.08	0.62	0.34	0.14	b.d.l.	0.07	b.d.l.	b.d.l.	b.d.l.
Tm	0.16	0.12	b.d.l.	0.09	0.05	b.d.l.	b.d.l.	b.d.l.	b.d.l.	0.02	b.d.l.
Yb	0.93	0.75	0.08	0.56	0.30	0.12	0.10	0.05	0.12	0.12	0.05
Lu	0.13	0.12	0.02	0.08	0.05	b.d.l.	0.02	0.01	0.02	0.02	b.d.l.
Sc	2.10	5.20	0.35	6.00	5.60	1.60	1.70	1.60	3.30	3.00	1.80
Total	58.36	80.19	15.15	53.69	31.42	16.75	12.67	10.34	14.95	13.63	7.56
ΣREE (ppm)	45.26	66.69	13.70	41.59	22.72	13.85	9.77	8.34	10.45	9.43	5.33
$(Eu/Eu^*)_{CN}$	1.57	2.27	7.14	2.96	4.01	4.40	5.15	11.16	5.87	5.08	9.32
$(La/Yb)_{CN}$	5.87	12.58	26.97	8.91	9.89	16.29	12.81	26.97	12.36	10.11	14.83
$(La/Nd)_{CN}$	1.89	2.26	2.69	1.75	1.98	2.24	1.84	2.76	2.37	2.05	1.94

Rock type	GN	GN	GN	GN	S	S	S	SD,a	SD,a	SD,a	SD,a
Sample	97-4	97-5	97-31b	98-68	98-40	99-20	Sy-25	98-201	98-103s	98-204	98-200
ppm											
Y	19.00	13.00	1.40	15.00	72.00	46.00	33.00	72.00	46.00	19.00	62.00
La	9.30	11.00	3.00	13.00	80.00	73.00	60.00	93.00	227.00	107.00	437.00
Ce	23.00	24.00	5.90	30.00	145.00	123.00	139.00	201.00	366.00	182.00	530.00
Pr	3.20	3.30	0.60	4.10	18.00	16.00	18.00	29.00	37.00	19.00	74.00
Nd	15.00	14.00	2.40	18.00	69.00	63.00	84.00	126.00	129.00	63.00	229.00
Sm	3.90	3.30	0.42	4.00	13.00	12.00	16.00	26.00	18.00	9.00	33.00
Eu	1.70	1.90	0.80	2.00	4.30	3.80	4.60	6.80	3.60	2.00	6.50
Gd	4.10	3.20	0.39	3.30	13.00	10.00	12.00	21.00	13.00	6.30	21.00
Tb	0.66	0.50	-	0.54	2.20	1.60	1.50	3.40	2.00	0.79	2.70
Dy	3.80	2.70	0.30	3.20	13.00	9.00	7.90	17.00	9.60	4.40	12.00
Ho	0.75	0.52	-	0.59	2.90	1.90	1.30	3.20	1.60	0.81	2.30
Er	2.10	1.40	0.21	1.60	8.20	4.90	3.20	8.20	5.00	2.20	5.30
Tm	0.32	0.20	0.04	0.24	1.30	0.68	0.41	1.10	b.d.l.	0.33	0.83
Yb	1.90	1.30	0.26	1.40	9.20	5.20	2.40	7.30	5.00	2.00	4.90
Lu	0.29	0.20	0.05	0.21	1.40	0.80	0.32	1.20	0.77	0.29	0.68
Sc	44.00	22.00	13.00	17.00	7.20	5.90	13.00	22.00	4.80	0.92	2.40
Total	133.02	102.52	28.77	114.18	459.70	376.78	396.63	638.20	868.37	419.04	1423.61
ΣREE (ppm)	70.02	67.52	24.37	82.18	380.50	324.88	350.63	544.20	817.57	399.12	1359.21
$(Eu/Eu^*)_{CN}$	1.30	1.79	6.04	1.68	1.01	1.06	1.02	0.89	0.72	0.81	0.75
$(La/Yb)_{CN}$	3.30	5.70	7.78	6.26	5.86	9.46	16.85	8.59	30.61	36.07	60.13
$(La/Nd)_{CN}$	1.20	1.52	2.42	1.40	2.24	2.24	1.38	1.43	3.40	3.40	3.40

Abbrevations: *A,w* white anorthosite; *A,ol* olivine anorthosite; *A,px* pyroxene anorthosite; *GN* leucogabbronorite; *S* syenite; *SD,a* altered syenodirite; *T* leucotroctolite.

Table 6. U-Pb analytical results for zircon from syenodiorite Ku-98-201, Swartbooisdrif, Namibia.

Sample[a]	Weight (mg)	Concentra (ppm)		^{206}Pb / ^{204}Pb Measured ratios[b]	Radiogenic Pb			Atomic ratios[c]			Apparent ages (Ma)[d]		
		U	Pb_{tot}		^{206}Pb	^{207}Pb	^{208}Pb	^{206}Pb / ^{238}U	^{207}Pb / ^{235}U	^{207}Pb / ^{206}Pb	^{206}Pb / ^{238}U	^{207}Pb / ^{235}U	^{207}Pb / ^{206}Pb
1	0.123	172	47.6	3560	73.3	6.43	20.27	0.2333	2.8198	0.0877	1352	1361	1375
2	0.194	135	41.3	370.8	74.37	6.52	19.11	0.2305	2.7861	0.0877	1337	1352	1375
3	0.145	167	46.5	658	73.92	6.49	19.59	0.2215	2.6792	0.0877	1290	1323	1377
4	0.106	161	45.1	1060	73.64	6.46	19.9	0.2292	2.7740	0.0878	1331	1349	1377

a Zircon concentrates were obtained using standard mineral-separation procedures and purified through separation by hand under the binocular microscope. All analyzed zircon crstalls had a prismatic habit, were pink, and smaller than 100 µm. ^{205}Pb-^{235}U mixed tracer was added before sample dissolution. All samples were dissolved with 52% HF in autoclaves at 220°C for four days, dried, and transfered overnight into chloride-form using 6N HCl. Ion-exchange chromatography follows the procedure described by Krogh

b Lead isotope ratios corrected for fractionation with 0.1% / a.m.u.

c Lead corrected for fractionation, blank, tracer contribution, and initial lead. During the measurement period

d Apparent ages were calculated using the constants of Jaffey et al. (1971) recommended by IUGS (Steiger

Table 7. Oxygen isotopic data of feldspar of the anorthosite and the felsic rock suites.

Rock type	Sample	Mineral	Textural relationship	$\delta^{18}O_{SMOW}$ mineral
White anorthosite	Ku-97-33	plagioclase	cumulus mineral	5.35
	Ku-97-33b	plagioclase	cumulus mineral	6.14
	Ku-97-33a	plagioclase	cumulus mineral	7.30
	Ku-98-45	plagioclase	cumulus mineral	2.36
	Ku-98-60	plagioclase	cumulus mineral	5.54
Pyroxene anorthosite	Ku-97-31	plagioclase	cumulus mineral	6.10
	Ku-97-92a	plagioclase	cumulus mineral	5.83
Leucogabbronorite	Ku-98-128	plagioclase	cumulus mineral	5.61
	Ku-98-222	plagioclase	cumulus mineral	5.99
Leucotroctolite	Ku-97-95	plagioclase	cumulus mineral	5.90
	Ku-97-95	olivine	interstitial	3.07
	Ku-97-105	plagioclase	cumulus mineral	3.19
	Ku-98-125	plagioclase	cumulus mineral	6.13
	Ku-98-220	plagioclase	cumulus mineral	5.63
Felsic rock suite	Ku-98-40	K-feldspar	phenocryst	7.22
	Ku-98-40	plagioclase	phenocryst	7.20
	Ku-99-13	K-feldspar	phenocryst	7.50
	Ku-99-20	K-feldspar	phenocryst	7.92
	Ku-99-21	K-feldspar	phenocryst	7.36
	Ku-99-21	plagioclase	phenocryst	7.52

Table 8. Sr and Nd isotope data for anorthosites and felsic rocks from NW Namibia.

Sample[a]	Region	GPS-coord.	Age[b] (Ma)	Sm[c] (ppm)	Nd[c] (ppm)	$^{143}Nd/^{144}Nd$[d] (meas)	$^{143}Nd/^{144}Nd$[e] (T)	εNd[e] (T)	Rb[c] (ppm)	Sr[c] (ppm)	$^{87}Sr/^{86}Sr$[d] (meas)	$^{87}Sr/^{86}Sr$[e] (T)	εSr[e] (T)	Nd model age (Ma)
Anorthosite (NW Namibia)														
White anorthosite														
Ku-97-30	Mine	19.505´´.48.110´´	1385	0.38	2.30	0.511810±5	0.51090	1.1	15.0	581	0.705317±7	0.70385	14	1713
Ku-97-33a	Mine	19.505´´.48.110´´	1385	0.26	1.40	0.511842±5	0.51095	2.0	10.0	480	0.705375±7	0.70413	18	1865
Dark anorthosite														
Ku-97-105	Zebra Mts.	25.100´´..38.500´´	1385	0.33	1.70	0.512021±5	0.51097	2.3	1.9	389	0.703423±7	0.70314	4	1692
Ku-98-219	Zebra Mts.	25.799´´. 40.032´´	1385	0.54	2.50	0.512132±5	0.51095	1.9	4.9	450	0.704266±7	0.70364	11	1754
Ku-98-227	Zebra Mts.	23.899´´..32.546´´	1385	0.12	0.69	0.511909±5	0.51094	1.7	0.7	500	0.703113±7	0.70303	2	1660
Ku-98-236	Zebra Mts.	09.705´´..33.700´´	1385	0.17	1.00	0.511919±5	0.51100	3.0	0.9	468	0.703052±7	0.70294	1	1613
Ku-98-208	Mine	20.861´´ .46.231´´	1385	0.35	1.60	0.512004±5	0.51096	2.2	2.1	515	0.703042±7	0.70284	-1	2010
Felsic rock suite (Swartbooisdrif area, NW Namibia)														
Altered felsic rocks														
Ku-98-201	Mine	21.367´´ .47.170´´	1377	26.0	126	0.512006±5	0.51088	0.4	1.5	197	0.707598±7	0.70718	61	1848
Ku-98-204	Mine	20.954´´ .47.155´´	1377	8.30	61.0	0.511733±5	0.51100	2.5	97.0	5000	0.708678±7	0.70761	67	1578
Ku-98-200	Mine	21.353´´ .47.109´´	1377	33.0	229	0.511776±5	0.51100	2.5	0.9	1301	0.706312±7	0.70627	48	1587
Felsic rocks unaffected by an alteration														
Ku-98-202	Mine	21.407´´ .47.161´´	1377	27.0	124	0.512029±5	0.51084	-0.4	18.0	541	0.706138±7	0.70430	20	1953
Ku-Sy-25	Mine	19.505´´ .48.110´´	1377	16.0	80.0	0.512067±5	0.51097	2.2	90.0	702	0.709539±7	0.70245	-6	1682

[a] Whole rock samples. Location as indicated in Fig. 2. Samples were dissolved with 52% HF for four days at 160°C on the hot plate. Digested samples were dried and taken up in 6N HCl. Sr and Nd were separated and purified using ion-exchange chromatography as described in Romer et al. (2005).

[b] Age from Fig. 6 and Drüppel et al. (2000).

[c] Concentrations of Nd and Sm were determined by ICP-MS using the procedures of Dulski (1994); Rb and Sr were determined by ICP-MS.

[d] The Nd isotopic composition was determined on a Finnigan MAT262 multi-collector mass-spectrometer using dynamic multicollection. Individual ratios were normalized to $^{146}Nd/^{144}Nd = 0.7219$, The Sr isotopic composition was determined on VG Sector 54-30 multi-collector mass-spectrometer using dynamic multicollection. Individual ratios were normalized to $^{86}Sr/^{88}Sr = 0.1194$ and $^{146}Nd/^{144}Nd = 0.7219$; analytical uncertainties are given at $2\sigma_m$ level. During the measurement period, reference material La Jolla and NBS 987 gave values of 0.511855 ± 8 (2σ, n = 15 samples) and 0.710246 ± 10 (2σ, n = 20 samples), respectively.

[e] Initial compositions and ε vales of Nd and Sr were calculated using the age of the complex and the following parameters and constants: $^{147Sm}\lambda = 6.54E\text{-}12\ y^{-1}$; $^{143}Nd/^{144}Nd_{CHUR}(0) = 0.512638$; $^{147S}m/^{144}Nd_{CHUR}(0) = 0.1967$; $^{87Rb}\lambda = 1.42E\text{-}11\ y^{-1}$, $^{87}Sr/^{86}Sr_{CHUR}(0) = 0.7045$; $^{87}Rb/^{86}Sr_{CHUR}(0) = 0.0816$. ε notation as in Jacobsen and Wasserburg (1979)